Pressure-induced multi-step and self-organized spin states in an electro-elastic model for spin-crossover solids

Mamadou Ndiaye, Kamel Boukheddaden

Pressure-induced multi-step and self-organized spin states in an electro-elastic model for spin-crossover solids

Mamadou Ndiaye[a,b], and Kamel Boukheddaden[a*]

[a] *Université Paris-Saclay, UVSQ, CNRS, GEMaC,*

45 Avenue des Etats Unis, 78035 Versailles, France

[b] *Université Cheikh Anta Diop de Dakar,*

Département de Physique, FST, BP 5005, Fann, Dakar, Sénégal

(Dated: April 15, 2022)

* Corresponding author. E-mail: kamel.boukheddaden@uvsq.fr

Abstract

The spin transition materials are known to exhibit a rich variety of behaviours under several stimuli, among which the pressure leads to major changes in their electronic and elastic properties. From the experimental point of view, thermal spin transitions under isotropic pressure showed transformations from (i) hysteretic to continuous transformations where the hysteresis width vanishes beyond some threshold pressure value; that is the conventional case. In several other cases very pathological and unexpected behaviours emerged, like (ii) persistent hysteresis under pressure; (iii) non uniform behavior of the thermal hysteresis width which first increases with pressure and then decreases and vanishes at higher pressures; (iv) also double step transitions induced by pressure are also often obtained, where the pressure triggers the appearance of a plateau during the thermal transition, leading to two-step transitions, and finally (v) other non-conventional re-entrant transitions, where the thermal hysteresis vanishes at some pressure and then reappears at higher pressure values are also observed. In the present theoretical study, we investigate this problem with an electro-elastic description of the spin-crossover phenomenon by solving the Hamiltonian by Monte Carlo technique. The pressure effect is here introduced directly in the lattice parameters, the elastic constants and ligand field energy. By considering spin state-dependence compressibility's, we demonstrate that a large panel of experimental observations can be qualitatively described with this model. Among them, we quote (i) the conventional pressure effect decreasing the hysteresis width, (ii) the unconventional cases with pressure causing a non-monotonous behaviour of the hysteresis width, (iii) re-entrant, as well as (iv) double step transitions accompanied with various types of spin state self-organization in the plateaus regions.

I. INTRODUCTION

Spin-crossover (SCO) materials are extensively studied due to their exceptional potential applications as sensor devices, molecular memories, displays, switches, etc [1–6] as well as for their fascinating fundamental aspects related to the coupling between their electronic and elastic structures. Such spin transition materials have been commonly investigated in iron(II) complexes with $3d^6$ configuration in octahedral symmetry. Their magnetic properties exhibit two kind of electronic configuration : paramagnetic high-spin state (HS) at high-temperature and diamagnetic low-spin state (LS) at low-temperature with their respective total spin, S=2 and S=0. From the optical and elastic point of view, the switching between HS and LS states, which is achieved by light [7–11], temperature [7, 8, 10, 12, 13], magnetic [14] or electric field [15], pressure [16–23] etc, is accompanied by a change of color which couples to a significant variation of the bond lengths between Fe and N atoms, which vary from $\sim$ 2.00 Å in the LS state to $\sim$ 2.2 Å in the HS state [7, 8, 10], leading to abrupt expansion by around 30% of the molecular volume of the coordination sphere [24]. In contrast, the expansion of the unit cell volume is $\sim$ 3-5 % which is [25], very small compared to that of the coordination sphere. This important difference of volume change results from the molecular crystal structure which absorbs a large part of the molecular volume expansion in the form of reorientations of the ligands and others local degrees of freedom which do not affect the unit cell volume [26]. In cooperative spin-crossover solids, the nucleation and the growth of the spin states during the spin transition arise from local volume expansions taking place at several regions in the lattice and their propagation is caused by their interference in the whole lattice (due to the long-range character of the emerging elastic interactions) resulting in a global volume expansion accompanied by significant deformation of the crystal lattice, which produces inhomogeneous mechanical stresses inside the system leading in some extreme cases to the breakdown of the crystals at the transition. From the experimental point of view, the investigations on the SCO molecular complexes benefited from a large panel of techniques, like x-ray diffraction, optical microscopy, colorimetry, Mössbauer and uv-visible spectroscopies, reflectively, photoluminescence [22, 24, 27–39] etc showing many features in the thermal properties of these materials such as gradual transition which follows the Boltzmann statistics, first-order transition with hysteresis, incomplete spin transitions with residual HS fraction at low-temperature, two-and multi-step transitions characterized

by intermediate plateaus in which the spin states are self-organized [40–48] etc. Theoretically, the mechanism behind all these behaviors are often investigated using macroscopic or microscopic descriptions such as the regular solutions model [49, 50] based on a thermodynamical approach where the interaction parameters related to the weak intermolecular interactions in iron(III) compounds are introduced in a phenomenological way, continuous medium model [51] which do not explicitly describe the particular micro-organization of the HS and the LS domains, and also Ising-like models [52–55] which propose a qualitative microscopic origin to the SCO phenomenon. Among the Ising-like models, we distinguish the vibrational models such as spin-phonon model [56] accounting for the coupling between spins and lattice phonons, which discard the macroscopic deformation of the lattice, and the models with anharmonic potentials such as Lennards-Jones pair potential [57] which contain a repulsive short-range and attractive long-range contributions or Morse potential [58], as well as mechanoelastic model [59], harmonic electroelastic model [60, 61] accounting for the deformation of the lattice. All these models are based on the interactions (short-and long-range) between the SCO neighbors atoms whose forces (weak or strong) evidence the degree of cooperativity of these systems. Indeed, in the electroelastic model [60, 62], the spin and the sites positions degree of freedom, which account for the lattice deformation during the spin transition, are combined to study the spatiotemporal and thermodynamics features of spin-crossover solids. This model reproduces many SCO behaviors and offers many extensions.

In the present investigations, we aim to study the effects of an isotropic applied pressure on the thermal spin transition and to analyze how does pressure impacts the spatiotemporal properties of 2D SCO systems modelled using the genuine electroelastic model. Experimental studies conducted on the spin-crossover materials under applied pressure gave a rich variety of behaviors, among which the more frequent one is the case where the hysteresis width decreases with increasing pressure causing its vanishing beyond a threshold pressure value, thus leading to a gradual transition, a situation which can be easily demonstrated from theory [26, 63–68]. The other case, still under debate, which can be considered as an anomalous behavior corresponds to that where the thermal hysteresis width increases when the pressure increases. This behavior was first reported experimentally by König et al. [69] more than 40 years ago. Later, others groups [26, 63, 70–72] reported this anomalous (non-conventional) behavior and another variety of behaviors, such as an hysteresis under

pressure which shifts at constant width to higher temperatures [71, 73], or vanishing small hysteresis which reappears at higher pressure [71, 74], which could be described as a reentrant phenomenon. Others spin transition behaviors with applied pressure can be found in the literature such as pressure-induced two-step transition [22, 75–77] but also the pressure can induce possible crystallographic transitions which then alters the intermolecular packing, or which even lead to symmetry breaking [76, 78–80], although most of the induced transformations are isostructural. However, all these behaviors under pressure are characterized by a common trend : the shift upwards of the transition temperature towards the higher values of temperature, due to the increase of the local ligand field strength and the compression of the molecular volume induced by the applied pressure. From a general point view, one may easily imagine the latter producing an inhomogeneous internal stresses inside the SCO lattice, acting locally on the bond lengths, and the elastic constants by promoting the local stabilization of the LS state from the electronic point of view, while the complex long-range elastic effects may generate elastic frustration inside the lattice .

Thus, to examine the interplay between the electronic and the elastic properties of the SCO materials under pressure, we investigated in this work the effect of the pressure on the general electro-elastic model using an original method. The pressure effect is directly put in the equilibrium bond lengths, in the elastic constants and in the ligand field in a linear way. Several situations are considered among which, the case of isotropic, and anisotropic pressure effect along the bond lengths. By monitoring the compressibilities parameters, we could reproduce a large part of the experimental observations cited above.

The paper is organized as follows: in Sec. II, we present the extended version of the 2D electro-elastic model for spin crossover solids by considering the distance parameters and elastic constants depending on the spin states and pressure. Then, from this model, we deduce the homogeneous electro-elastic model equivalent to Ising model combining long-range ferroelastic and short-range antiferroelastic interactions. Sec. III is devoted to the presentation and the discussion of the various thermal dependencies of HS fractions and spatiotemporal organizations emerging from the simulations under pressure. In Sec. IV, we conclude and outline the possible extensions of the present work.

II. THE MODEL

The spin-crossover solids are described well by the electro-elastic model which takes into account for the electronic and elastic properties in a 2D square lattice of total number sites, $N \times N$, depicted in Fig. 1. Here, each SCO molecule representing a lattice site is associated with a fictitious spin state, $S_i = \pm\ 1$, where $S_i = +1$ and $S_i = -1$ define the HS state and LS state, respectively. In this 2D SCO lattice, every site is connected to its four neighbors by harmonic springs where the elastic constants and the equilibrium distances depend on the spin states highlighting the local elastic field distortion which accompanies the local variation of the molecular volume during the spin conversion. The Hamiltonian describing such 2D system is given by,

$$\begin{aligned} H = & \sum_i (\Delta - k_B T \ln g) S_i \\ & + \sum_{i,j} A(S_i, S_j)[r_{ij} - R(S_i, S_j)]^2 \\ & + \sum_{i,k} B(S_i, S_k)[d_{ik} - d(S_i, S_k)]^2 \end{aligned} \tag{1}$$

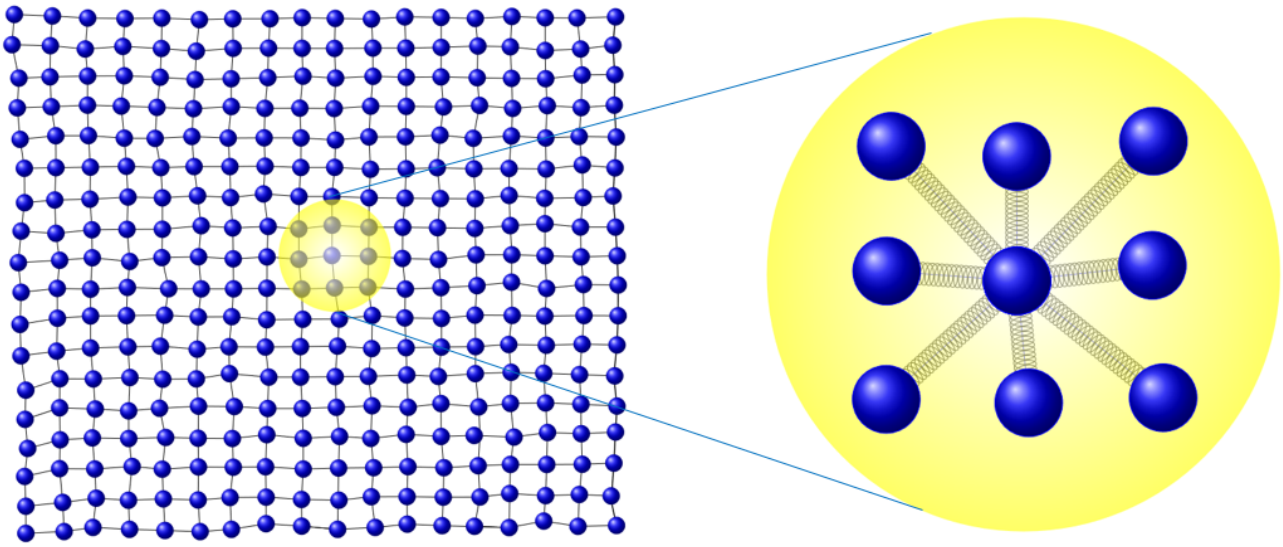

Figure 1: Left: 2D elastic configuration lattice with nearest neighbors and next-nearest neighbors atoms linked by harmonic springs. Right : schematic view of the lattice interactions of a SCO atom in the center with its four nn atoms and four nnn atoms.

The first term of Eq. (1) is the effective temperature–dependent energy gap between the

LS and HS states. It contains the effective ligand field energy, $\Delta - k_B T \ln g$ contribution, arising from the difference of ligand fields, Δ, in the HS and LS states at T=0 K and, the entropic contribution originating from the electronic and vibrational degeneracy ratio, $g = g_{HS}/g_{LS}$, between the HS and LS states. The second and the third terms describe the elastic interactions between the nearest (nn) and next-nearest neighbors (nnn) of SCO units, respectively.By considering two nn (nnn) nodes of the 2D discretized lattice, connected by springs and located at sites (i, j) and (i', j'), their respective instantaneous distance r_{ij} (r_{ik}) is $r(i, j|i', j') = |\vec{r}(i', j') - \vec{r}(i, j)|$ $[r(i, k|i', k') = |\vec{r}(i', k') - \vec{r}(i, k)|]$, whose indexes are $i' = i, j' = j \pm 1$ and $i' = i \pm 1, j' = j$ $(i' = i \pm 1, k' = k \pm 1)$. The equilibrium bond length between two nn (resp. nnn) atoms which interact via elastic springs is denoted $R_0(S_i, S_j)$ (resp. $d_0(S_i, S_k) = \sqrt{2}R_0(S_i, S_k)$. Let us denote by, R_0^{HH}, R_0^{HL} and R_0^{LL}, the equilibrium distances between nn HS-HS, HS-LS and LS-LS sites, we then have $R(+1, +1) = R_0^{HH}$, $R(+1, -1) = R(-1, +1) = R_0^{HL}$ and $R(-1, -1) = R_0^{LL}$. In the same way, we consider that the elastic constant of a spring linking two nn (resp. nnn) atoms depends on their spin states. So, for HS-HS, HS-LS and LS-LS configurations, A_{HH}, A_{HL} and A_{LS} (resp. B_{HH}, B_{HL} and B_{LS}) represent the nn (resp. nnn) elastic constants. It is straightforward to derive the general expressions of the nn (resp. nnn) equilibrium bond lengths, $R_0(S_i, S_j)$ (resp. $d_0(S_i, S_k)$) and the nn (resp. nnn) elastic constants, $A(S_i, S_j)$ (resp. $B(S_i, S_k)$), as function of the spin states S_i and S_j under the following forms:

$$R_0(S_i, S_j) = R_0^{HL} + \frac{\delta R}{4}(S_i + S_j) \tag{2}$$

$$A_0(S_i, S_j) = A_0 + A_1(S_i + S_j) + A_2 S_i S_j \tag{3}$$

$$B_0(S_i, S_k) = B_0 + B_1(S_i + S_k) + B_2 S_i S_k \tag{4}$$

where, the parameters A_i(i=0, 1, 2) and B_i(i=0, 1, 2) write under the general form:

$$\begin{aligned} X_0 &= \frac{X_{HH} + X_{LL} + 2X_{HL}}{4}, \\ X_1 &= \frac{X_{HH} - X_{LL}}{4} = \frac{\delta X}{4}, \\ X_2 &= \frac{X_{HH} + X_{LL} - 2X_{HL}}{4}, \end{aligned} \tag{5}$$

and $R_0^{HL} = \frac{R_0^{HH} + R_0^{LL}}{2}$ with $\delta R_0 = R_0^{HH} - R_0^{LL}$ is the lattice misfit between the HS and LS phases. Owing to the square symmetry of the lattice, the bond length of nnn sites are obtained by multiplying the latter by $\sqrt{2}$ which gives $d_0(S_i, S_k) = \sqrt{2}R_0(S_i, S_k)$. In

general, the Hamiltonian (1) can be re-written under the form of an Ising-like model (see ref. [52]) containing long-range effective field-like contribution and exchange-like interactions mixing local short-and long-range contributions. Next, we will consider how to introduce the pressure effect in this Hamiltonian.

A. Derivation of the electroelastic model under pressure

In this section, we investigate the effect of an external pressure on the elastic thermodynamics and spatiotemporal properties of the present 2D system. The expression of the Hamiltonian under an applied isotropic pressure is given by,

$$\begin{aligned} H_{elas} = & \sum_{i} \left(\Delta - k_B T \ln g\right) S_i \\ & + \sum_{i,j} A(S_i, S_j) \left[r_{ij} - R(S_i, S_j)\right]^2 \\ & + \sum_{i,k} B(S_i, S_k) \left[d_{ik} - d(S_i, S_k)\right]^2 + PV \end{aligned} \tag{6}$$

where in the last term the quantity, V, represents the system's "volume". To anticipate the results of Monte Carlo simulations and to understand how the pressure affects the equilibrium lattice parameters, we first solve the problem in the context of homogeneous lattice, by considering a uniform bond length through the network. Thus, the instantaneous distances, r_{ij} between nn and d_{ik} between nnn become x and $x\sqrt{2}$, respectively. The minimization of the total elastic energy of the Hamiltonian (6) in the 3D case, where $V = Nx^3$, with respect to the variable x, by solving the equation, $\frac{\partial H_{elas}}{\partial x}$=0 leads at mechanical equilibrium, for relatively low-pressure, to the following general expression of the equilibrium bond length with pressure,

$$x_{eq}(P) = x^0_{eq}(1 - \beta P), \tag{7}$$

where the calculations details and the expressions of the equilibrium bond length for zero pressure, x^0_{eq}, and the compressibility, β, are given in Sec. A of the Appendix.

It is worth to mention that the derived linear pressure-dependence of x_{eq} expression (7) is in fair agreement with several experimental results of literature, which showed a linear decrease of the lattice parameters in the limit of reasonably low-pressure values, typically less than 1 GPa for SCO materials [18, 22, 63, 81, 82]. On the other hand, the compressibility factor, for a lattice spacing a, defined as $\beta = -\dfrac{d\ln\left[a\right]}{dP}$, has been estimated for SCO materials

by Laisney et al. [22] at ~ 0.003 kbar^{-1}. As will be seen later, the used β values in the simulations are in fair agreement with these experimental data.

We note in passing, for the reader interested in the homogeneous elastic model and its possible isomorphism with an Ising-like Hamiltonian combining competitive long- and short-range interactions, that we provide in Sec. B of the Appendix the detailed expressions of the interactions parameters as well as those of the effective field with respect to pressure in the case of pressure-independent nn and nnn elastic constants.

From now, we re-express the Hamiltonian (6) by introducing directly the pressure-dependence in the ligand field energy (Δ_{eff}), the equilibrium bond lengths (R) as well as in the elastic constants (A and B). By so doing, we consider only the mechanical equilibrium states, which means that we assume that, under pressure, the structure relaxes faster than the spin states. Including these ingredients, leads to the electroealstic Hamiltonian (8), which will be solved by MC simulations. It should be recalled, in passing, that in this model where all molecules are connected by springs, in the HS and LS states, all the springs are unstressed : the elastic energy is then equal to zero and the distance between two nn molecules (HS-HS or LS-LS) corresponds to equilibrium bond lengths. When the SCO lattice undergoes a thermal spin transition from HS (resp. LS) to LS (resp. HS), a compression (resp. expansion) of the molecular volume leading to a shortening (resp. stretching) of the bond lengths due to the local displacements of the nodes, takes place. The expression of the effective Hamiltonian of the 2D elastic square lattice under the effect of an external pressure is given as follows,

$$\begin{aligned} H = & \sum_i (\Delta + \alpha P - k_B T \ln g) S_i \\ & + \sum_{i,j} A(S_i, S_j, P)[r_{ij} - R(S_i, S_j, P)]^2 \\ & + \sum_{i,k} B(S_i, S_k, P)[d_{ik} - d(S_i, S_k, P)]^2. \end{aligned} \tag{8}$$

In Eq. (8), the effect of the pressure leads to the renormalization of the effective ligand field as we have already explained, which shifts the equilibrium temperature towards higher temperatures following the Clausius-Clapeyron relation, $\frac{dT}{dp} = \frac{\Delta V}{\Delta S}$. From the effective ligand field, $\Delta_{eff} = \Delta + \alpha P - k_B T \ln g$, the new expression of the transition temperature writes,

$$T_{eq}(P) = T_{eq}^0 + \frac{\alpha P}{k_B \ln g}, \tag{9}$$

where $T_{eq}^0 = \frac{\Delta}{k_B \ln g}$ is the equilibrium temperature at zero applied pressure.

B. The expressions of the elastic constants and bond lengths under pressure

From the pressure-dependence of the relaxed lattice parameter given in (7), we could derive the general expressions of the equilibrium nn bond lengths between the HS-HS, HS-LS and LS-LS neighbours, which write,

$$R_{HH} = R_0^{HH}(1 - \beta_{nn}^{HH} P), R_{HL} = R_0^{HL}(1 - \beta_{nn}^{HL} P), R_{LL} = R_0^{LL}(1 - \beta_{nn}^{LL} P), \quad (10)$$

and we define those of nnn as,

$$d_{HH} = \sqrt{2} R'_{HH}, d_{HL} = \sqrt{2} R'_{HL}, d_{LL} = \sqrt{2} R'_{LL}. \quad (11)$$

It is quite easy to demonstrate that the general expressions of the nn (resp. nnn) pressure-dependence of the bond lengths, $R(S_i, S_j, P)$ (resp. $d(S_i, S_k, P)$), and elastic constants, $A(S_i, S_j, P)$ (resp. $B(S_i, S_k, P)$), appearing in Hamiltonian (8), whatever their spin states , can be re-written using the previous zero-pressure expressions (2)-(4) as follows,

$$R(S_i, S_j, P) = R_0(S_i, S_j)[1 - \beta_{nn}(S_i, S_j)P], \quad (12)$$

$$d(S_i, S_k, P) = d_0(S_i, S_k)[1 - \beta_{nnn}(S_i, S_k)P] \quad (13)$$

and

$$A(S_i, S_j, P) = A_0(S_i, S_j)[1 + \gamma_{nn}(S_i, S_j)P], \quad (14)$$

$$B(S_i, S_k, P) = B_0(S_i, S_k)[1 + \gamma_{nnn}(S_i, S_k)P], \quad (15)$$

where, β_{nn} (resp. β_{nnn}) and γ_{nn} (resp. γ_{nnn}) stand for the nn (resp. nnn) bond and elastic constant compressibilities, respectively.

C. A predictive analytical elastic approach

As a first-step for understanding of the pressure effect on the different contributions of the model, we re-express (8) under the form of an Ising-like model. By considering a homogeneous instantaneous bond length between nn ($r_{ij} = x$) and nnn ($r_{ik} = x\sqrt{2}$) SCO, we find after some simple development

$$H = h(P) \sum_i^N S_i + J^{nn}(P) \sum_{ij} S_i S_j + J^{nnn}(P) \sum_{ik} S_i S_k + C(P), \quad (16)$$

where, $C(P) = E_{cohesion} + C_0$ is the cohesion energy, whose expression is given in Sec. B of the Appendix.

The exchange-like parameters, $J^{nn}(P)$, $J^{nnn}(P)$ and the field-like contribution $h(P)$ write as follows

$$J^{nn}(P) = J_0^{nn} + J_1^{nn}(x - R_{HL}) + J_2^{nn}(x - R_{HL})^2, \tag{17}$$

$$J^{nnn}(P) = J_0^{nnn} + J_1^{nnn}(x - R'_{HL}) + J_2^{nnn}(x - R'_{HL})^2, \tag{18}$$

where,

$$\begin{aligned} J_0^{nn} &= 2\left[A_0(P) + A_2(P)\right]\left(\frac{\delta R}{4}\right)^2, \\ J_1^{nn} &= -4A_1(P)\left(\frac{\delta R}{4}\right), \\ J_2^{nn} &= A_2(P) \end{aligned} \tag{19}$$

and,

$$\begin{aligned} J_0^{nnn} &= 4\left[B_0(P) + B_2(P)\right]\left(\frac{\delta R'}{4}\right)^2, \\ J_1^{nnn} &= -8B_1(P)\left(\frac{\delta R'}{4}\right), \\ J_2^{nnn} &= 2B_2(P). \end{aligned} \tag{20}$$

Eqs. (17) and (18) clearly show that the local exchange-like interactions, $J^{nn}(P)$ and $J^{nnn}(P)$, which are globally positive, thus favoring antiferroelastic interactions, contain short-range terms, J_0^{nn} and J_0^{nnn}, inducing intrinsic frustration along the nn and nnn lattice parameters and additional elastic contributions having linear and quadratic forms. On the other hand, the local field-like term, $h(P)$, writes as follows,

$$\begin{aligned} h(P) = (\Delta + \alpha P - k_B T \ln g) + h_{0,1} + h_{0,2} + h_{1,1}(x - R_{HL}) + h_{1,2}(x - R_{HL})^2 \\ + h_{2,1}(x - R'_{HL}) + h_{2,2}(x - R'_{HL})^2, \end{aligned} \tag{21}$$

where,

$$h_{0,1} = 4zA_1(P)\left(\frac{\delta R}{4}\right)^2, h_{0,2} = 8zB_1(P)\left(\frac{\delta R'}{4}\right)^2, \tag{22}$$

$$h_{1,1} = -2z[A_0(P) + A_2(P)]\left(\frac{\delta R}{4}\right), h_{2,1} = -4z[B_0(P) + B_2(P)]\left(\frac{\delta R'}{4}\right), \tag{23}$$

$$h_{1,2} = zA_1(P), h_{2,2} = 2zB_1(P), \tag{24}$$

where, z is the lattice coordination number.

The parameter, $h(P)$ also contains two parts, which are the effective field contribution including the effect of the pressure and an additional field-like elastic contribution, which stabilize the HS or LS state due to their long-range nature. We notice that the elastic part of $h(P)$ has a linear and quadratic contribution too.

The minimization of the elastic energy (8) with respect to x in order to get the mechanical equilibrium is done by solving the equation $\frac{\partial E_{elas}}{\partial x}$=0 leading to the general expression of the equilibrium bond length:

$$x_{eq} = \frac{\sum_{i,j} A(S_i, S_j, P)R(S_i, S_j, P) + 2\sum_{i,k} B(S_i, S_k, P)R'(S_i, S_k, P)}{\sum_{i,j} A(S_i, S_j, P) + 2\sum_{i,k} B(S_i, S_k, P)}. \tag{25}$$

This analytical approach, which merits to be studied for its own, show the complexity of this model, although the pressure is introduced in a simple way into the Hamiltonian, by injecting it in the expressions of the lattice parameter and elastic constants. This development allows a mean-field analysis of Hamiltonian (16) combining nn and nnn interactions, which is out the scope of the present work. In the next section, we will solve exactly Hamiltonian (8), combined with Eqs. (10)-(15), using a Monte Carlo procedure running on spins and lattice positions.

III. MONTE CARLO SIMULATIONS

The Monte Carlo procedure used to investigate the thermodynamic properties of the 2D square lattice under isotropic applied pressure is performed on the spin and the lattice positions. Here, we consider a 2D square lattice of size $N \times N = 30 \times 30$, with free boundary conditions, where each site of spin S_i is elastically connected by springs to its nearest and next-nearest neighbors. The system is initially prepared in the HS phase by fixing all spins to $S_i = +1$ and all nn lattice bond lengths to R_0^{HH}. Simulations based on the Metropolis algorithm are performed as follows: (i) we randomly select a site i and update its spin state following the Metropolis criterion. (ii) Whatever the result, accepted or rejected spin flip,

we perform another MC process by displacing each lattice position randomly with a small quantity (typically $\delta x \simeq 0.05$, $\delta y \simeq 0.05$) compared to the lattice parameter distance ($\simeq 1$) in order to minimize the system's elastic energy. We update all lattice positions by MC 10 times in order to reach the mechanical equilibrium. Then, we call randomly another spin site and we repeat this sequential procedure until visiting all spin sites. When all spin sites have been visited once, we call this 1 MC step (MCS). To determine the thermal properties of the system, we first cool down from the higher temperatures to 1 K and then warmed up to the initial temperature, with 1 K increment. At each temperature, we perform 10^3 MCS to reach the equilibrium state and we use 10^3 other MCS for the statistics.

A. Model parameters

The Monte Carlo simulations are realized using, as much as possible, realistic values for the model parameters. Thus, the ligand-field energy is taken as $\Delta = 450$ K for the ligand field energy, the degeneracy ratio is set to $g = 150$ ($\ln g = 5$) leading to an entropy change at the transition $\Delta S \simeq 41$ J.K^{-1}.mol^{-1} in good agreement with experimental data of heat capacity measurements [83]. The transition temperature is easily deduced as, $T^0_{eq} = \dfrac{\Delta}{k_B \ln g} = 90$ K. The values of the nn equilibrium bond lengths are taken equal to $R_0^{HH} = 1.2$ nm between two HS sites and $R_0^{LL} = 1.0$ nm between two LS sites and so $R_0^{HL} = \dfrac{R_0^{HH} + R_0^{LL}}{2} = 1.1$ nm.

For the elastic part, the average elastic constants were fixed to $1.5 \times 10^4 - 2 \times 10^4$ K/nm^2 (see Table I) leading to an estimated average bulk modulus, $G \simeq A/ < R > \sim 8$ GPa ($< R >$ is the average lattice parameter), which is in fair agreement with available experimental data of Brillouin scattering performed on the single crystal of $[Fe(ptz)_6](ClO_4)_2$ estimating the bulk modulus in the range $5 - 20$ GPa [71, 84].

The set of used parameter values is summarized in Table I, which in addition to the values of the equilibrium bond lengths, elastic constants, also includes the bond-compressibility coefficients used along the numerical simulations.

Table I: Nearest neighbors (nn) and next-nearest neighbors (nnn) equilibrium bond lengths, elastic constants and compressibility coefficients values used in the Monte Carlo simulations for the different electronic configurations. The values of the compressibility of the nnn bond length is changed along the studies related with the thermal properties under pressure.

Spin state configurations	HH	HL	LL
nn distances (nm)	R_0^{HH}=1.2	R_0^{HL}=1.1	R_0^{LL}=1.0
nnn distances (nm)	$R_0^{HH}\sqrt{2}$	$R_0^{HL}\sqrt{2}$	$R_0^{LL}\sqrt{2}$
nn elastic constants ($\times 10^4 K/nm^2$)	A_0^{HH}=0.9	A_0^{HL}=1.46	A_0^{LL}=2.0
nnn elastic constants ($\times 10^4 K/nm^2$)	B_0^{HH}=1.1	$B_0^{HL} = B_0^{HH}$	$B_0^{LL} = B_0^{HH}$
nn Bond length compressibility ($kbar^{-1}$)	β_{nn}^{HH}=0.1	$\beta_{nn}^{HL} = \frac{\beta_{nn}^{HL}+\beta_{nn}^{LL}}{2}$	β_{nn}^{LL}=0.05
nnn Bond length compressibility ($kbar^{-1}$)	β_{nnn}^{HH}	$\beta_{nnn}^{HL} = \frac{\beta_{nnn}^{HL}+\beta_{nnn}^{LL}}{2}$	β_{nnn}^{LL}
nn elastic constant compressibility ($kbar^{-1}$)	γ_{nn}^{HH}=0.1	$\gamma_{nn}^{HL} = \frac{\gamma_{nn}^{HH}+\gamma_{nn}^{LL}}{2}$	γ_{nn}^{LL}=0.2
nnn elastic constant compressibility ($kbar^{-1}$)	$\gamma_{nnn}^{HH} = \gamma_{nn}^{HH}$	$\gamma_{nnn}^{HL} = \frac{\gamma_{nnn}^{HH}+\gamma_{nnn}^{LL}}{2} = \gamma_{nn}^{HL}$	$\gamma_{nnn}^{LL} = \gamma_{nn}^{LL}$

IV. RESULTS AND DISCUSSIONS

In this section, we present the results of the thermal investigations on a 2D square lattice of size $N \times N = 30 \times 30$ with free boundary conditions under various values of the isotropic applied pressure. We consider here the case of small applied pressures between 0 and 5 kbar with $\alpha = 30$ K/kbar. We initially prepare the lattice in the HS state by putting all spins $S_i = +1$ and fixing all nn distances equal to R_0^{HH}. Then, we monitor the pressure during the thermal transition for various values of the nnn bond length compressibility. Different thermal and pressure-dependence behaviors are then found according to β_{nnn} values. Among them conventional and non-conventional pressure effects that have been reported in experimental literature are found. All the others simulation parameters are given in the Sec. III A.

A. Conventional pressure effect on spin crossover hysteresis

The first case we consider here is that of the thermal spin transition with hysteresis width vanishing as the pressure increases. This conventional case is obtained by considering the HS phase more compressible than the LS phase. For that, we set the nnn bond length compressibilities $\beta_{nnn}^{HH} = 0.04$, $\beta_{nnn}^{LL} = 0.03$, and $\beta_{nnn}^{HL} = 0.035$ kbar^{-1}, which assumes that the HS state is softer than the LS. We depict in Figs. 2a and 2b the thermal-dependence of the HS fraction and nn bond length for different values of applied pressure. Figure 2a shows that, for $P = 0$, the system undergoes an usual first-order transition at $T_{eq} \sim 84$ K($< T_{eq}^0 = 90$) accompanied with a thermal hysteresis of width $\Delta T \sim 38$ K. Increasing the pressure decreases the width of the hysteresis which vanishes at $P = 3$ kbar, leading to a gradual spin transition which persists until P=5 kbar. This disappearance of the thermal hysteresis width is accompanied with a shift of the transition temperature towards higher temperatures due to the increase of the effective ligand field energy. One can also remark that the shape of $n_{HS}(T)$ becomes less sharper. Figure 2b shows that when the pressure increases, an important drop of the nn bond lengths of the HS state (from 1.2 to 0.85 nm) and those of the LS state (from 1.0 to 0.8 nm) takes place. This reduction in the bond length changes between the LS and the HS states is at the origin of the weakening of the strength of elastic interactions which are proportional to the elastic energy, $(A + 2B)(r_{HS} - r_{LS})^2$, resulting from the lattice parameter misfit.

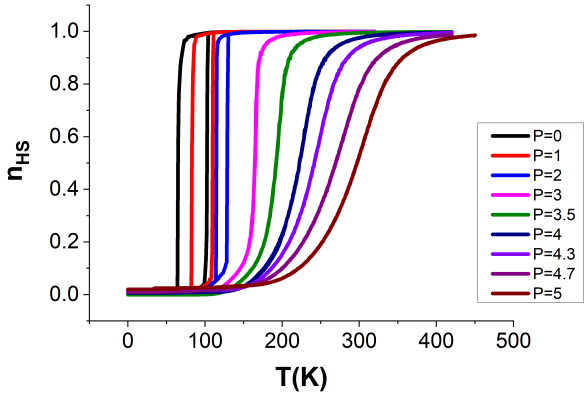

(a)

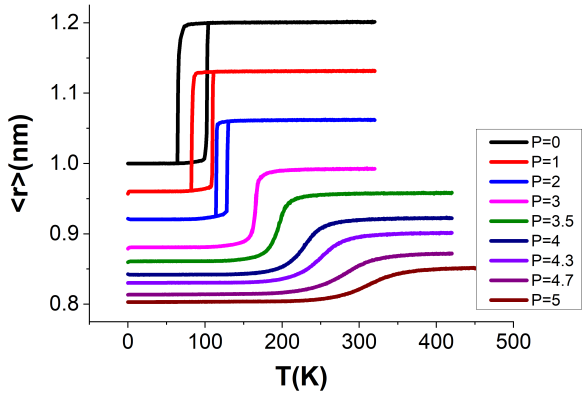

(b)

Figure 2: Thermal-dependence of the (a) HS fraction and (b) the average bond length for different applied pressure values ranging from 0 to 5 kbar for nnn compressibilities, $\beta_{nnn}^{HH} = 0.04$, $\beta_{nnn}^{LL} = 0.03$, and $\beta_{nnn}^{HL} = 0.035$ kbar^{-1} (for nn compressibilities see Table (I). Under pressure, the first-order transition transforms a gradual one beyond the threshold value of pressure $P^* \simeq 2.5$ kbar.

Fig. 3a depicts the evolutions with respect to pressure of the square of the lattice misfit between the HS state and the LS state, $< \Delta r >^2 = (< r_{HS} > - < r_{LS} >)^2$, and the thermal hysteresis width, ΔT, and in Fig. 3b that of the equilibrium temperature, T_{eq}. Figure 3a shows that when the pressure increases, the hysteresis width, ΔT, and Δr^2 decrease and become null beyond some threshold pressure value. When the pressure increases ΔT decreases linearly until $P^* \simeq 2.5$ kbar beyond which it cancels, while $< \Delta r >^2$ which is correlated to ΔT decreases slightly until $P \sim 4.6$ kbar and becomes null for higher pressures

values. On can notice in Fig. 3b that the thermal transition increases with pressure following a parabolic law. This non-linearity of the transition temperature with respect to pressure is due to the contribution of the elastic part (nn and nnn elastic interactions) leading to a behavior quite different from the usual one where the thermal transition increases linearly with the pressure following the Clausius-Clapeyron relation. Indeed, the decrease of the hysteresis width, ΔT, leading to the appearance of the gradual transition is related to the lowering of the cooperativity of the system. In fact, the increase of the pressure shortens the distances which weakens the strength of the elastic interactions through the decrease of the elastic energy barrier between the HS and LS states. A simple explanation of the P^2-dependence of T_{eq} can be obtained from Eq. (21). Considering the simple assumption based on that the equilibrium temperature of the system results from the average value of the ligand field, the thermal transition is obtained by setting $h = 0$ in Eq. (21),

$$\begin{aligned} T_{eq} = T_{eq}^0 + \frac{\alpha P}{k_B \ln g} + \frac{1}{k_B \ln g}[h_{0,1} + h_{0,2} + h_{1,1}(\overline{x_{eq}} - R_{HL}) + h_{1,2}(\overline{x_{eq}} - R_{HL})^2 \\ + h_{2,1}(\overline{x_{eq}} - R'_{HL}) + h_{2,2}(\overline{x_{eq}} - R'_{HL})^2] \end{aligned} \tag{26}$$

where, $\overline{x_{eq}} = \frac{x_{eq}^{HS} + x_{eq}^{LS}}{2}$. At the first-order, T_{eq} depends linearly on pressure. At the second order, the contributions $(\overline{x_{eq}} - R_{HL})^2$ come into play by adding P^2 terms.

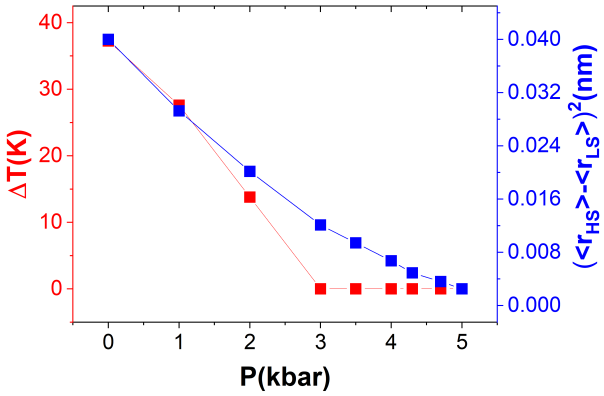

(a)

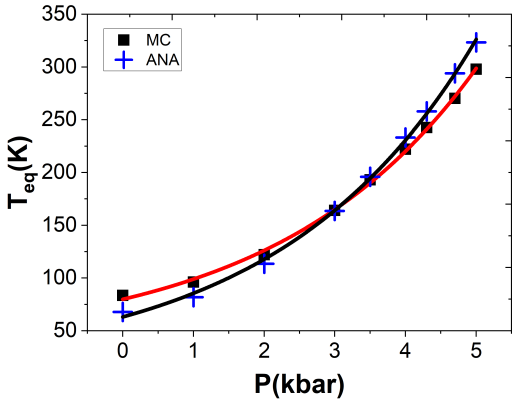

(b)

Figure 3: (a) Pressure-dependence of the hysteresis width, ΔT (K), and the HS/LS lattice misfit, $< \Delta r >^2 = (< r_{HS} > - < r_{LS} >)^2$, derived from the data of Fig. 2b showing a decreasing of these two quantities. (b) Pressure-dependence of the equilibrium temperature, T_{eq}, resulting from the MC data of the Fig. 2a showing an increase of the thermal transition following parabolic law. The values of the compressibility parameters as well as the others parameters used for the simulations are the same as those of the Fig. 2.

The inspection of the spatial distribution of the spin states depicted in the Figs. 4a, 4b, 4c shows the existence of different types of organizations. For $P = 0$ and $P = 2$, for which we got the first-order transitions, the corresponding snapshots denote domain nucleation from the four corners and a propagation inside the lattice on cooling. On heating a similar behavior is obtained, although the nucleation starts preferentially from the surface for $P = 2$ kbar. For $P = 3.5$ (Fig. 4c), the nucleation starts everywhere under the form of

"multidoplet" or ramified structure on cooling and as well as on heating. The absence of the spin domains is related to the lowering of the strength of the elastic interactions compared to the magnitude of the effective ligand field energy which is significantly enhanced by the pressure effects. As a result, the system becomes weakly cooperative (see corresponding gradual transition in Fig. 2) which prevents the appearance of macroscopic spin domains at the transition. On the other hand, this spatial disorder of the spin states is associated to the non-homogeneous decrease of the nn and nnn bond lengths along the $x-$and $y-$directions and the diagonals. Indeed, the rate of change of the nn bond lengths under pressure is greater than that of the nnn bond lengths due to the weak values of the β_{nnn} compressibility. We also remark that the spatial organization of the spin states is correlated to deformations and twisting of the lattice which are associated with the large misfit between HS and LS $\sim 20\%$ and to the choice of the compressibilities of the nnn elastic constants.

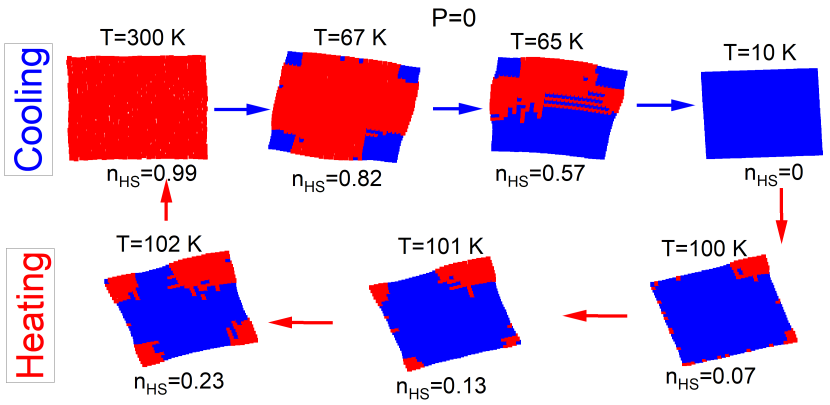

(a)

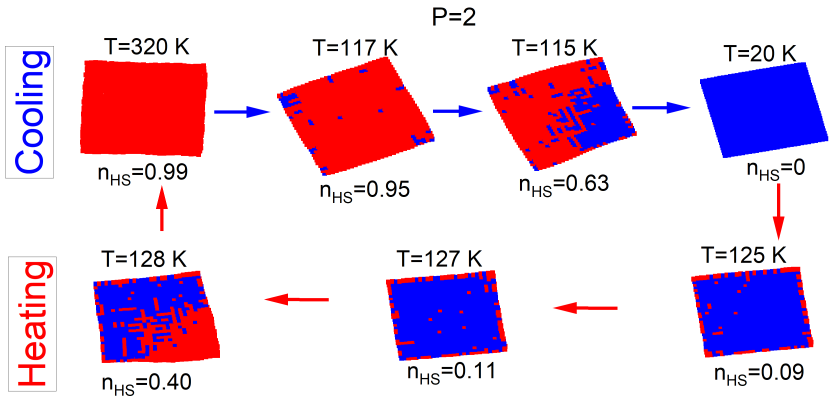

(b)

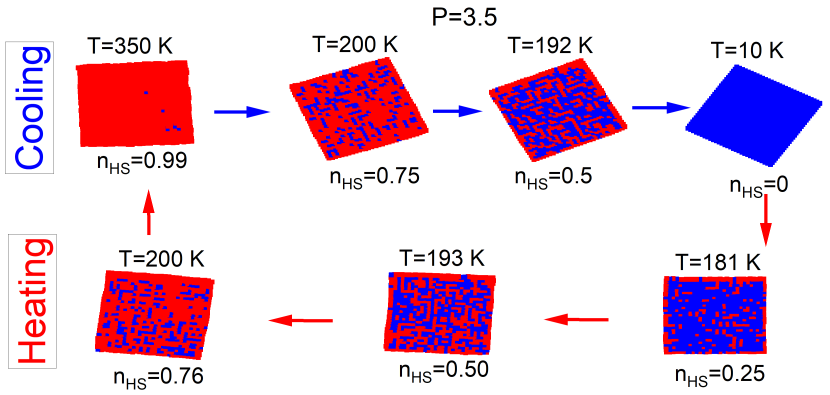

(c)

Figure 4: Selected snapshots showing the self-organisation of the spin states (red=HS, blue=LS) along the thermal transitions of Fig. 2 for the pressure values $P = 0$ (a); $P = 2$ (b) and $P = 3.5$ kbar (c). See text for more explanations.

B. A thermal hysteresis surviving to pressure effects

The second step of the present investigations concerns the case of SCO systems undergoing a first order-transitions with hysteresis loops shifting upwards and slowly vanishing when the pressure increases. This behavior corresponds to a non-conventional case which is obtained here by considering negative compressibilities associated to the nnn HS and LS bond lengths, $\beta_{nnn}^{HH} = \beta_{nnn}^{LL} = -0.03$. All others parameters values are kept unchanged and are the same as those used in the previous cases. Figs. 5a and 5b summarize the thermal evolution of the HS fraction and the average lattice spacing under pressure up to 5 kbar, respectively. Figure 5a shows that although the thermal hysteresis width decreases with pressure, it does not disappear even for $P = 5$ kbar. The main reason of this behavior is found in Fig. 5b which shows a slight change of the HS and LS lattice parameter under pressure, which then only slightly reduces the strength of the elastic interactions which depend on $(< r_{HS} > - < r_{LS} >)^2$. Compared to the case of Fig. 2a, where the hysteresis totally vanished at $P = 3$ kbar, here the chosen compressibility values allow a bigger amplitude of hysteretic behavior under pressure, as observed experimentally in some SCO materials [71, 85].

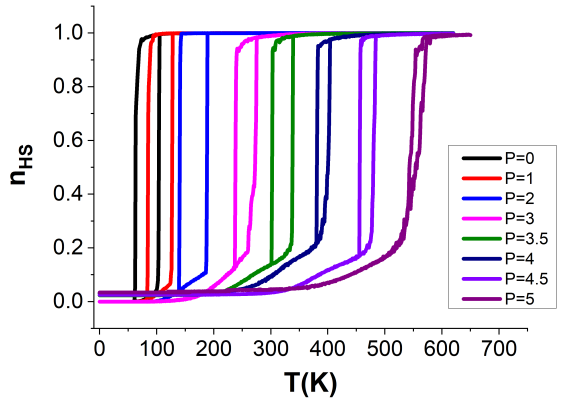

(a)

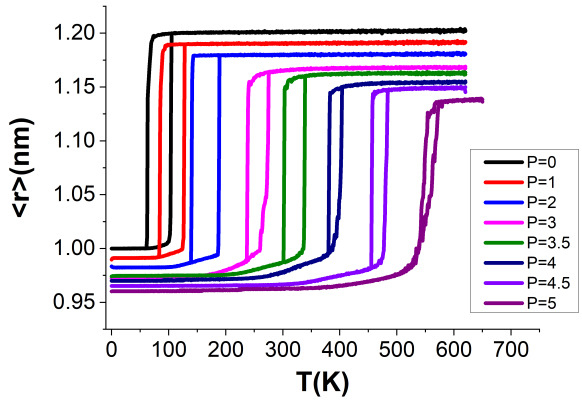

(b)

Figure 5: Thermal-dependence of the (a) HS fraction, n_{HS}, and (b) the average bond length, $< r >$, for different applied pressure values ranging from 0 to 5 kbar for the values of the nnn compressibilities, $\beta_{nnn}^{HH} = -0.03$, $\beta_{nnn}^{LL} = -0.03$, and $\beta_{nnn}^{HL} = -0.03$. Under pressure, the first-order transition with hysteresis survives towards the higher temperatures. All the others simulation parameters are the same as Fig. 2 except those of the nnn compressibilities and are given in the Table I.

We represent in Fig. 6a and Fig. 6b the pressure-dependence of the respective thermal hysteresis width and the square difference of the average distance between HS and LS, $< \Delta r >^2 = (< r_{HS} > - < r_{LS} >)^2$, as well as the transition temperature, T_{eq}. Fig. 6a shows the presence of two regimes for ΔT and $< \Delta r >^2$ when the pressure increases. For small P values ($P < 1.5$ kbar) ΔT and $< \Delta r >^2$ remain almost constant while beyond 2 kbar both

quantities decrease with pressure in a correlated way, which confirms the fact that $< \Delta r >^2$, which represents the square of the lattice misfit squared is one of the relevant parameters describing the strength of the elastic interactions.

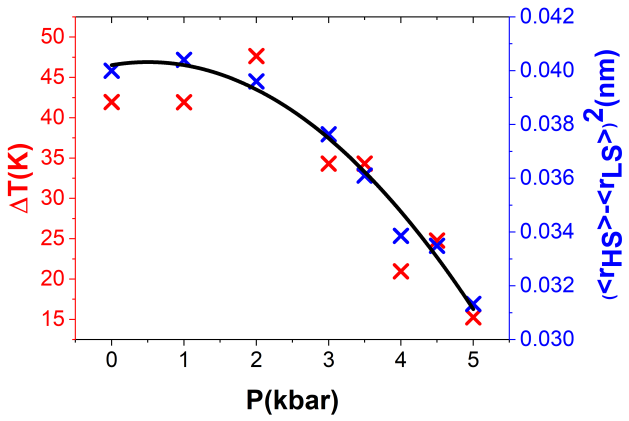

(a)

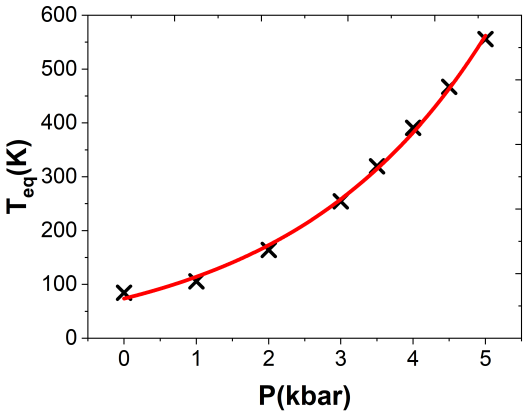

(b)

Figure 6: Pressure-dependence of (a) hysteresis width, ΔT (K) (red dots), and square of the lattice misfit, $< \Delta r >^2 = (< r_{HS} > - < r_{LS} >)^2$ (blue dots), showing a parabolic decrease of both parameters and (b) the equilibrium temperature, T_{eq} also showing a parabolic increase. All these data are derived from those of Fig. 5a and Fig. 5b.

C. Pressure-induced reentrant phase transition

Among the various behaviors induced by the effect of the applied pressure in SCO solids, the case of the reentrance phenomenon reported in some experimental investigations [86]

is interesting and puzzling. This phenomenon is studied in physics of phase transition, particularly in magnetism and ferroelectricity [67] and is generally characterized by the non-monotonous behavior of the order parameter. In SCO materials, reentrance effects induced by an applied pressure might be attributed to the existence of a pressure-induced structural phase transition. Usually, this transition is triggered beyond some threshold pressure value, which leads to a significant change in the material properties. In the present study, we do not include any structural phase transition induced by pressure. In contrast, we look for reentrant effects by adapting the pressure-dependence of the lattice compressibilities. At this end, we set the following relations between the nn and nnn compressibilities in the three spin configurations: $\beta_{nnn}^{HH} = \beta_{nn}^{HH}$, $\beta_{nnn}^{HL} = \beta_{nn}^{HL}$ and $\beta_{nnn}^{LL} = \beta_{nn}^{LL}$ with $\beta_{nnn}^{HH} > \beta_{nnn}^{HL} > \beta_{nnn}^{LL}$. Figures 7a and 7b depict the respective thermal-dependences of the high spin fraction, n_{HS}, and average distance, $< r >$, for different values of pressure. In Fig. 7a, we represent the curves in 3D axis only for three values of the pressure for helping the reader to better see the reentrance effect as function of the pressure. For $P = 0$ and 1 kbar (low pressure), the SCO system undergoes a first-order transition with hysteresis which transforms into a gradual transition for 2 and 3 kbar while the hysteresis reappears again for $P = 4 - 5$ kbar. This reentrant thermal transition is directly related to the thermal dependence of $< r >$, given in the Fig. 7b, which shows that when the pressure increases, the nn average distances of the HS ($< r_{HS} >$) and LS ($< r_{LS} >$) states, decrease with the same rate until $P = 3$ kbar where $< r_{HS} >=< r_{LS} >= 0.85$ nm. Beyond this threshold value, $< r_{HS} >$, continues to decrease more than $< r_{LS} >$, due to its stronger compressibility. When $< r_{LS} >$ exceeds the value of $< r_{HS} >$, the thermal hysteresis reappears again for a pressure value located in the range $2.5 - 3$ kbar. To well understand this behavior one must analyze the dependence of the average value of the misfit parameter, $< \Delta r >=< r_{HS} > - < r_{LS} >$ with respect to the pressure. Considering a linear dependence with pressure, the misfit parameter $< \Delta r >= \Delta_R^0 - (R_0^{HH}\beta_{nn}^{HH} - R_0^{LL}\beta_{nn}^{LL})P$, where $\Delta_R^0 = (R_0^{HH} - R_0^{LL}) = 0.2$ nm, one can see that for the small pressure values $< \Delta r >> 0$ while for the higher values of the pressure $< \Delta r >< 0$. Thus, the pressure induces in this case a change of the sign of $< \Delta r >$ beyond the threshold value of the pressure, $P_{th} = \frac{\Delta_R^0}{(R_0^{HH}\beta_{nn}^{HH} - R_0^{LL}\beta_{nn}^{LL})} \simeq 2.86$ kbar obtained by setting $< \Delta r >= 0$ in the previous expression. This value is in excellent agreement with the obtained one from MC simulations in Fig. 8a, where ΔT vs P is reported. Above $P = 3.5$ kbar the hysteresis reappears as shown in Fig. 8a, where the width, ΔT, is here also well

correlated with $< \Delta r >^2$.

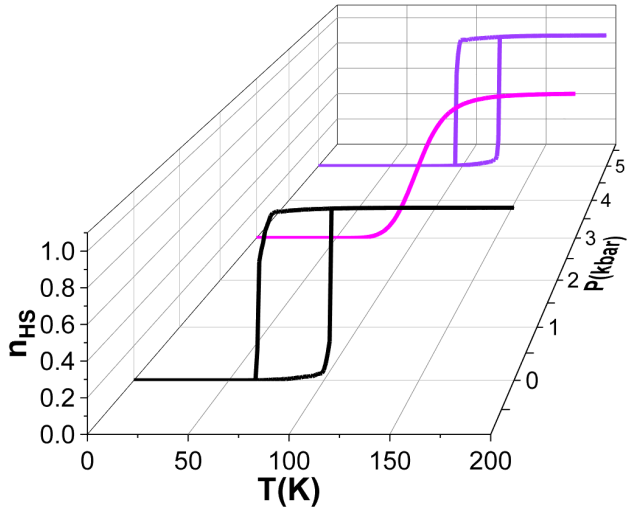

(a)

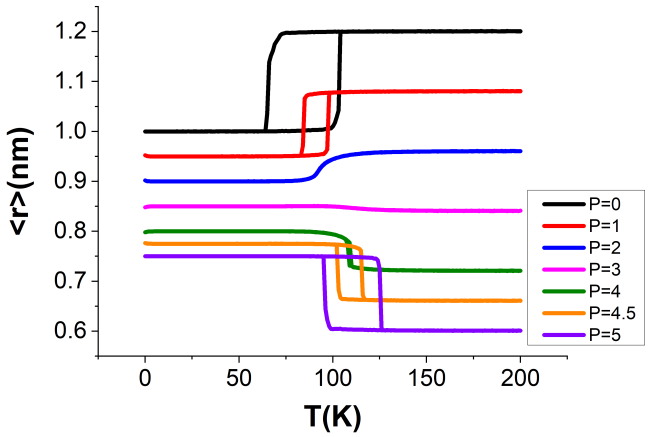

(b)

Figure 7: Thermal-dependence of the (a) HS fraction, n_{HS}, and (b) the average bond length, $< r >$, for different values of the applied pressure showing a reentrant phase transition. The values of the nnn distance compressibilities of the HH, HL and LL, are $\beta_{nnn}^{HH} = 0.1$, $\beta_{nnn}^{LL} = 0.05$, and $\beta_{nnn}^{HL} = 0.075$. All other parameters including the nn compressibilities are the same as those of Fig. 2.

Interestingly the pressure-dependence of the transition temperature, $T_{eq}(P)$, given in Fig. 8b shows a linear behavior which contrasts with the results of Fig. 6. Indeed, by constraining $\beta_{nn}^{HH} = \beta_{nnn}^{LL}$, $\beta_{nn}^{LL} = \beta_{nnn}^{LL}$, and $\beta_{nn}^{HL} = \beta_{nnn}^{LL}$, the nonlinear elastic part of the thermal

transition in Eq. (26) cancels and the transition temperature becomes, $T_{eq}(P) = T^0_{eq} + \frac{\alpha P}{k_B \ln g}$, where T^0_{eq} is the initial temperature at $P = 0$, and $\alpha = 30$ K/kbar. For higher pressure values, the situation could change and one can except an appearance of nonlinear effects.

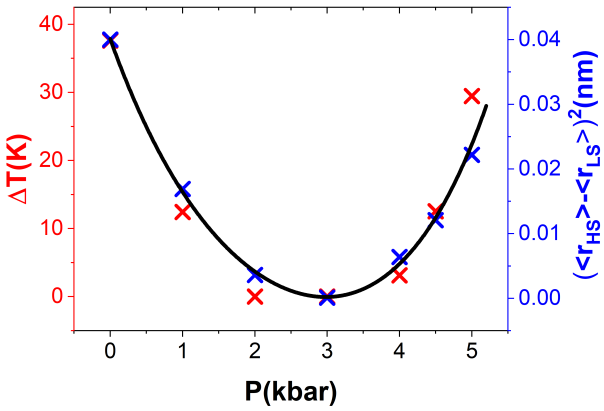

(a)

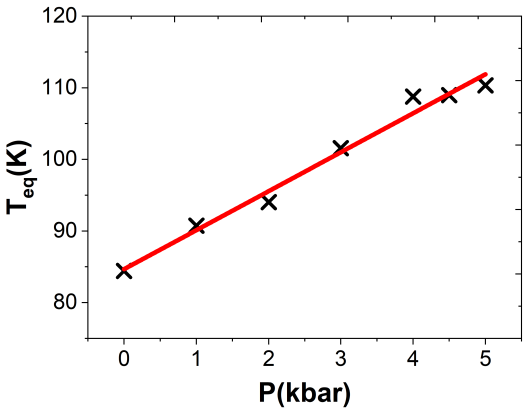

(b)

Figure 8: (a) Pressure-dependence of the width, $\Delta T(K)$, (in red dots) of the thermal hysteresis and $< \Delta r >^2 = (< r_{HS} > - < r_{LS} >)^2$, derived from the Fig. 7b, showing a close correlation between them. (b) Pressure-dependence of the transition temperature, T_{eq}, showing a linear behaviour. All results are, derived from Fig. 7a.

Selected snapshots showing the spatial organization of the spin states on cooling and on heating along the thermal hysteresis of Fig. 7a are summarized in the supplemental material (SM) as Figs. SM1, SM2 and SM3. For $P = 0$ (Fig. SM1), we notice the usual formation of the domains from the corners related to the effective ligand field, h, which

has a long-range ferroelastic character. When the pressure increases from 0 to 3 kbar, the self-organization changes due to the weak cooperative character of the system imposed by the pressure. Thus, for $P = 2$ kbar (Fig. SM2), a random nucleation of the LS states inside the HS states ("multidoplets") is obtained. For $P = 5$ kbar (Fig. SM3), on cooling and heating the nucleation starts from the edges and corners and evolves under the form of single domains which grow and propagate inside the lattice.

D. Pressure-induced two-step transition

Here, we investigate, the case where the pressure induces two-step spin transitions as often observed in experimental literature [75–77]. The values of the nnn bond compressibility parameters of the HH, LL and HL states used to obtain this behavior are : $\beta_{nnn}^{HH} = 0.04$, $\beta_{nnn}^{LL} = 0.05$, and $\beta_{nnn}^{HL} = 0.045$ kbar^{-1}. We depict in Figs. 9a and 9b the thermal-dependence of the HS fraction, n_{HS}, and average bond length, $< r >$, at different pressure values. Figure 9a shows a clear transformation of a first-order transition to a two-step transition when the pressure is increased. The crossover between the two behaviours takes place at $P = 2.3$ kbar to which corresponds two hysteretic spin transitions with equilibrium temperatures, $T_{eq} = 120$ K and $T_{eq} = 110$ K, separated by a small intermediate plateau around $n_{HS} = 0.5$. Increasing the applied pressure up to $P = 4$ kbar, transforms the previous two "hysteretic" first-order transitions to two gradual spin- transitions (for $P = 3.5$ K, for example) located at $T_{eq} = 160$ and 200 K, with an enlarged intermediate plateau width. Figure 9b shows the corresponding thermal behavior of the nn average distance, $< r >$, which contracts as the pressure increases. To understand the physical origin of this two-step transition, one has to focus on the chosen compressibility values. Indeed, in the present case, we considered a nnn bond compressibility of LS state bigger than that of HS state, while we have the opposite tendency for the nn bonds. Thus, when the pressure is applied to a square HS unit cell, nn distances decrease under pressure with a slope $\beta_{nn}^{HH} = 0.1$, while that of nnn, less compressible, decrease with a slope $\beta_{nnn}^{HH} \simeq 0.04$. These "antagonist" effects produce a frustration in the system which stabilizes intermediate antiferro-like states. Figures 10a and 10b summarize the pressure-dependence of the average nn bond lengths in HS ($< r_{HS} >$) and LS ($< r_{LS} >$) and that of the equilibrium temperature, T_{eq}, respectively. We see that $< r_{HS} >$ and $< r_{LS} >$ linearly decrease as function of P from 1.2 nm to 0.96 nm (HS)

and from 1.0 nm to 0.8 nm (LS) with a greater slope for the HS state which has a stronger compressibility. On the other hand, the transition temperature, T_{eq} first linearly increases in the pressure range 0-1 kbar corresponding to the region of one-step transition and then splits into two linear branches denoted T_{eq}^{up} and T_{eq}^{down} corresponding to the two-step transition region. Here, the slope of the curve $T_{eq}^{up}(P)$ is bigger than that of $T_{eq}^{dwn}(P)$ due to the difference of compressibilities between the HS and LS states. Overall, this linear increase of thermal transition under the applied pressure is in agreement with the Clapeyron relation.

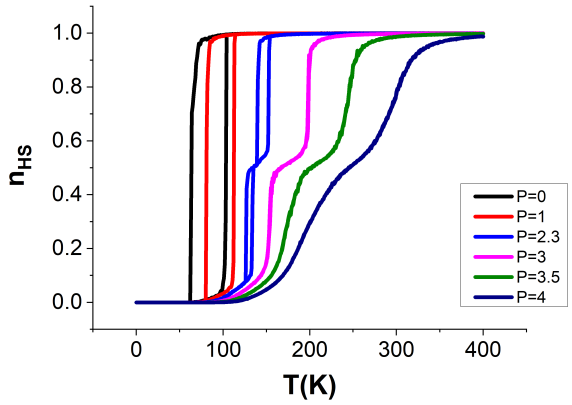

(a)

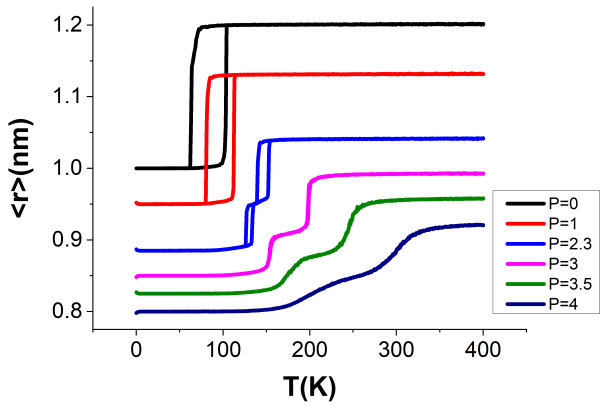

(b)

Figure 9: Thermal-dependence of the (a) HS fraction and (b) average nn bond length for different values of the applied pressure with the nnn fixed compressibilities values, $\beta_{nnn}^{HH} = 0.04$, $\beta_{nnn}^{LL} = 0.05$, and $\beta_{nnn}^{HL} = 0.045$ kbar^{-1}, showing the occurrence of a double step transition with two "hysteretic" transitions for $P = 2.3$ kbar which become two gradual ones for stronger pressure values. All others parameters are the same as those of Fig. 2.

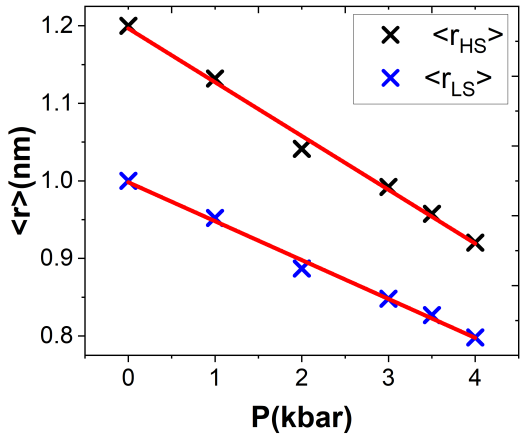

(a)

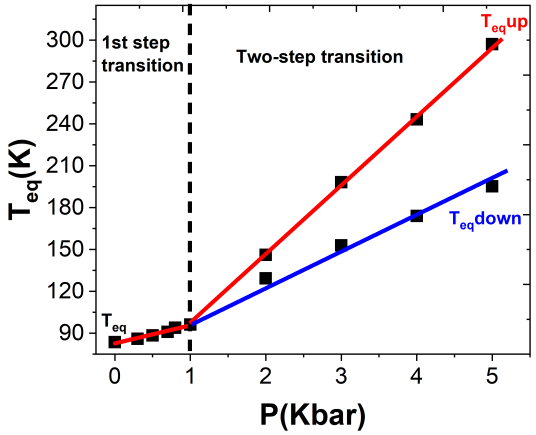

(b)

Figure 10: (a) Evolution of the average nn lattice parameter in HS and LS states showing a linear decreasing behavior with the pressure. (b) Pressure-dependence of the transition temperatures of Fig. 9a showing the regions of one step and two-step transitions. The results of both panels are derived from Fig. 9.

To analyze the spatial distribution of the HS and LS states in the case of two-step transitions, we plot in Figs. 11a and 11b some selected snapshots along the thermal transition curves of Fig. 9 for $P = 2.3$ and 3.5 Kbar. The case $P = 0$ is not shown here, because it is the same as those of previous figures where spin domains started from the corners. For $P = 2.3$ and 3.5 Kbar, clear self-organizations of the spin states around the plateau regions are obtained. On cooling from HS, small LS chains emerge from the borders, whose lengths

increase as we approach the center of the plateau region, forming a macroscopic complex structure made of alternating HS and LS stripes along $x-$and $y-$directions for $n_{HS} \simeq 0.5$. These labyrinths stripes disappear when the system approaches the HS or the LS state. This labyrinth formation can be understood by the fact that there is no anisotropy effect taken into account in the model, since the compressibility parameters along $x-$and $y-$directions are equivalents although different from those along the diagonals. In this case the system has tendency to stabilize HS and LS stripes along $x-$and $y-$directions simultaneously causing this irregular (disordered) spin state organization in the lattice, which is enhanced by the contribution of the diagonals since the nnn compressibility of the HS state is lower than that of the LS state leading to the frustration of the system.

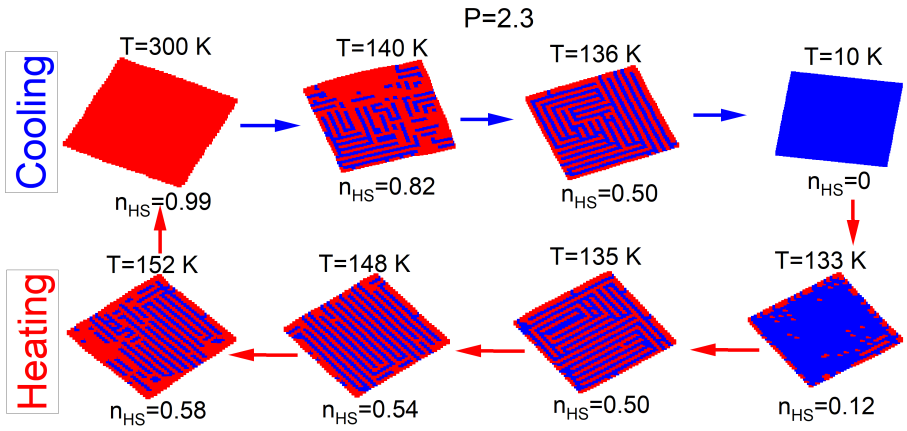

(a)

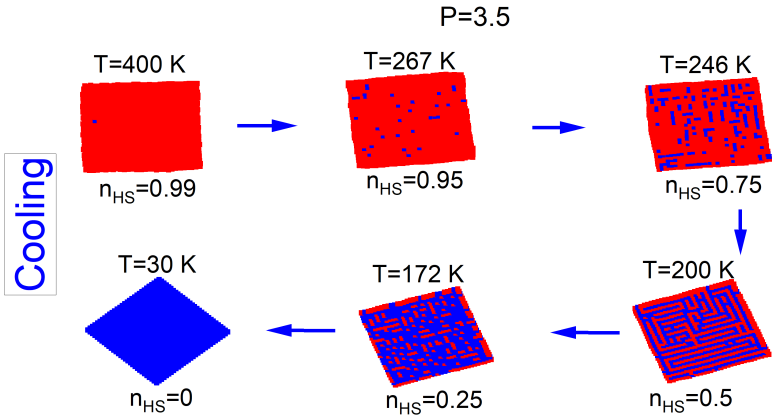

(b)

Figure 11: Spatial organization of the HS (red) and LS (blue) states during the thermal transition of Fig. 9a showing the occurrence of self-organization for (a) $P = 2.3$ and (b) $P = 3.5$ kbar, stabilizing a macroscopic structure under the form of labyrinths made of alternating HS and LS stripes in the plateau region.

E. Anisotropy-induced stripes phases along $x-$ or $y-$directions

Until know we considered the same compressibility parameters between the nn bond lengths along the $x-$ and $y-$directions. To investigate the effect of the anisotropy on thermal and spatiotemporal properties in the case of pressure-induced double step transition (Fig. 9), we set different nn compressibility values, β_{nn}^{X} and β_{nn}^{Y} along $x-$ and $y-$directions, respectively. All other parameters used in the simulations are the same as those of Fig. 9.

In first case, $\beta_{nn}^{X} > \beta_{nn}^{Y}$, we consider the values of the nn compressibility in the HH, HL and LL states along $x-$direction, $\beta_{nn}^{X,HH} = 0.1$, $\beta_{nn}^{X,LL} = 0.05$, and $\beta_{nn}^{X,HL} = 0.075$, greater than those along $y-$direction, $\beta_{nn}^{Y,HH} = 0.03$, $\beta_{nn}^{Y,LL} = 0.01$, and $\beta_{nn}^{Y,HL} = 0.02$. The MC simulations lead in this cases to two-step thermal dependence of the HS fraction of Fig. 12a, obtained for the applied pressure $P = 3.5$ kbar. Two "hysteretic" first-order transitions centered around at $T_{eq}^{+} = 127$ K and $T_{eq}^{-} = 75$ K separate a large plateau of ~ 50 K width at $n_{HS} \sim 0.5$. Selected snapshots along the thermal hysteresis depicted in Fig. 12b show well organized successive HS, LS stripes perfectly organized along $y-$direction with the presence of defects at the surface. When we consider exactly the opposite case ($\beta_{nn}^{Y} > \beta_{nn}^{X}$), we obtain the results of Fig. 12c and the corresponding snapshots given in Fig. 12d which exhibits a perfect stripes ordering along $x-$ direction. Thus, by considering different nn compressibilities along $x-$ and $y-$ directions, $\beta_{nn}^{X} > \beta_{nn}^{Y}$ (or $\beta_{nn}^{Y} > \beta_{nn}^{X}$), we obtained a total disappearance of the labyrinths observed in Figs. 11a and 11b, at the benefit of perfect stripes, which means that we left the degeneracy between these two directions. In fact, for $\beta_{nn}^{X} > \beta_{nn}^{Y}$ (resp. $\beta_{nn}^{Y} > \beta_{nn}^{X}$), the nn bond lengths are more compressible in the $x-$ direction (resp. $y-$direction) than in the $y-$ direction (resp. $x-$direction) with $\beta_{nn}^{X,HH} > \beta_{nn}^{X,LL}$ ($\beta_{nn}^{Y,HH} > \beta_{nn}^{Y,LL}$) . In contrast, the compressibilities of the nnn bond lengths along the diagonals are taken so as to have $\beta_{nnn}^{HH} < \beta_{nnn}^{LL}$. The 2D system will be then frustrated and the minimization of the elastic energy excess results in the stabilization of alternate of 1D HS and LS strings along the $y-$ direction or $x-$direction only.

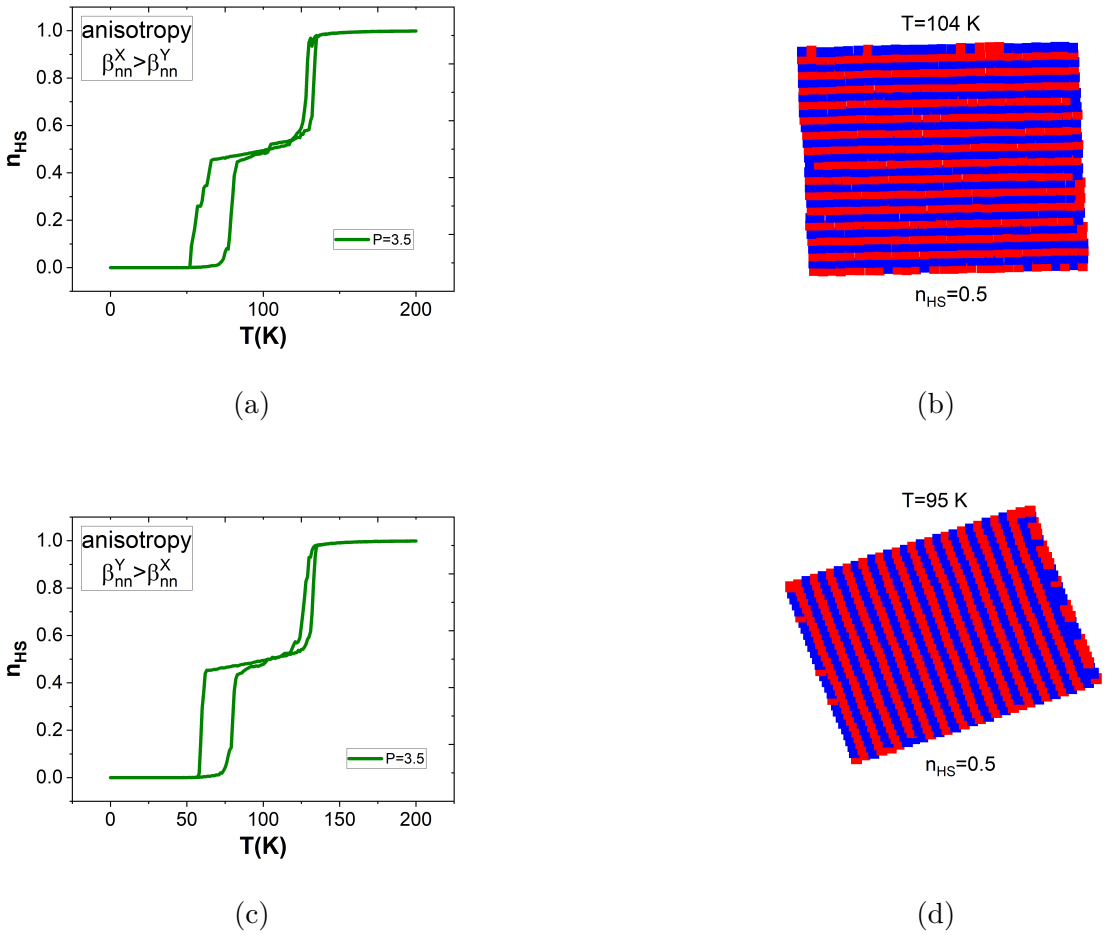

(a) (b)

(c) (d)

Figure 12: Thermal-dependence of the HS fraction, n_{HS}, for an applied pressure $P = 3.5$ kbar showing a two-step behavior made of first-order transitions obtained for $\beta_{nn}^X > \beta_{nn}^Y$ (a) and $\beta_{nn}^Y > \beta_{nn}^X$ (c). Corresponding selected snapshots in the plateau region showing a perfect self-organization of successive HS and LS stripes along $y-$ (b) and $x-$directions (d) at $n_{HS} = 0.5$. The other parameter values (except β_{nn}^X and β_{nn}^Y) are the same as those of Fig. 9.

V. ISOTHERMAL PIEZO-SWITCHING

Here, we investigate the effect of the pressure on a SCO system in isothermal conditions. The idea is to control the spin transition by pressure and to look for the condition of baro-switching as well as for the lattice transformation along this transitions triggered by an istropic pressure. At this end, several situations are tested for different temperatures,

corresponding to the various behaviours obtained in the previous sections.

A. Conventional pressure effect on spin crossover hysteresis

We start with the situation of Fig. 2, where the applied pressure only shifts the spin-crossover transition to higher temperatures and gradually decreases the width of the thermal hysteresis. The simulations are performed by starting from the HS phase of Fig. 2 for $P = 0$ at fixed temperature $T = 90$ K exactly situated in the bistable region (the middle of the thermal hysteresis) and another one located in the monostable HS phase region ($T = 200$ K). The obtained results are summarized in Fig. 13 for the case $T = 90$ K and Fig. 14 for $T = 200$ K, where in both figures we included the pressure-dependence of the HS fraction and that of the average nn bond length, $< r >$. Figure 13 exhibits a sharp baroswitching reflecting the first-order transition and the bistable nature of the lattice at $T = 90$ K, while a gradual and continuous baroswitching is obtained at $T = 200$ K, in agreement with the stable nature of the initial HS state at $P = 0$. On the other hand, the linear dependence of the lattice parameters in Fig. 13b and Fig. 14b from both sides of the pressure-induced spin transition region, results from the simple assumption of Eq. (10). In agreement with the first-order and gradual pressure-induced transitions of Figs. 13 and 14, their corresponding lattice configurations along the transitions, given in 13c and 14c, show clear domain nucleation for the first-order transition and ramified growth for the gradual one similarly with the previous domain growth in thermally-induced phase transitions. It is interesting to remark the sharp character of the pressure-induced transition of Fig. 13a without presence of an hysteresis while the latter is present in the thermal transition of Fig. 2. The main reason of the absence (or very small value of) the hysteresis width is related to the change of the average lattice parameter, $< r >$, at the transition (see Fig. 13b). Due to the linear dependence of the equilibrium lattice distances on pressure, and to the difference of compressibilities of HS and LS states, the average HS lattice parameter is significantly decreased by pressure while that of LS state is less affected (lower compressibility). As a result the lattice misfit Δr in the lattice spacing (~ 0.15 nm) is significantly lowered compared to that of the thermal transition (0.2 nm) which then causes the reduction of the hysteresis width.

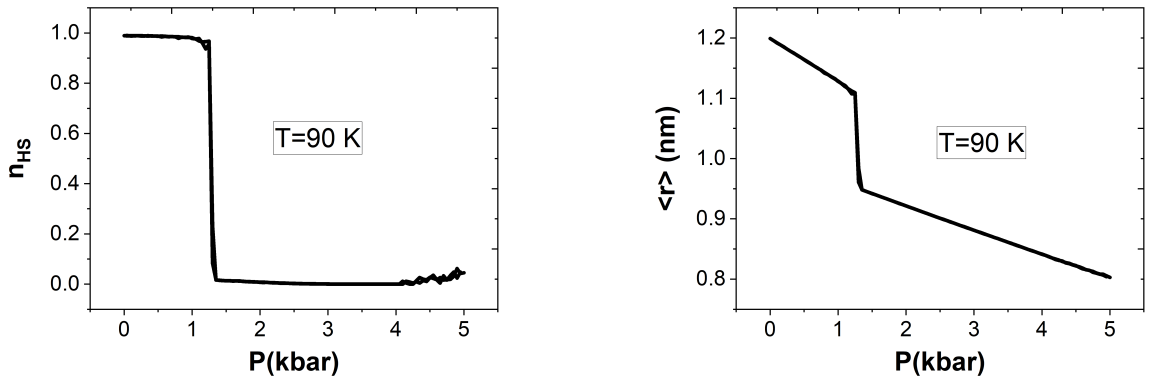

(a)

(b)

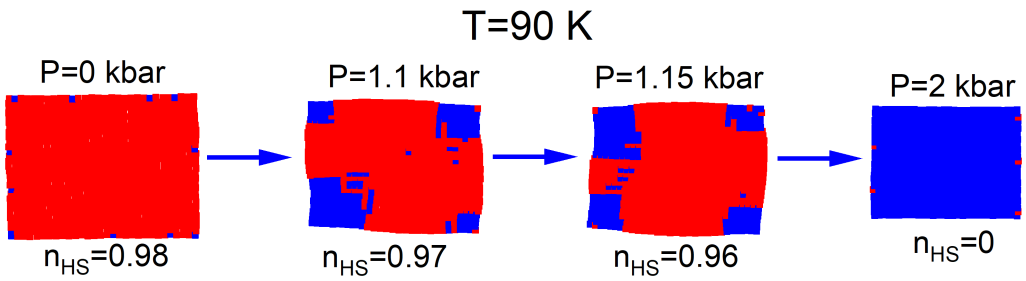

(c)

Figure 13: Pressure-dependence of the (a) HS fraction, n_{HS}, and (b) average distance, $< r >$, at constant temperature $T = 90$ K showing a first-order HS $\rightarrow$ LS transition. (c) Selected snapshots showing a formation of LS (blue area) domains inside the HS (red area) phase along the pressure-induced spin transition. The parameter values (except T) are the same as those of Fig. 2. The absence of hysteresis loops is due to the decrease of the lattice misfit at the transition between HS and LS states.

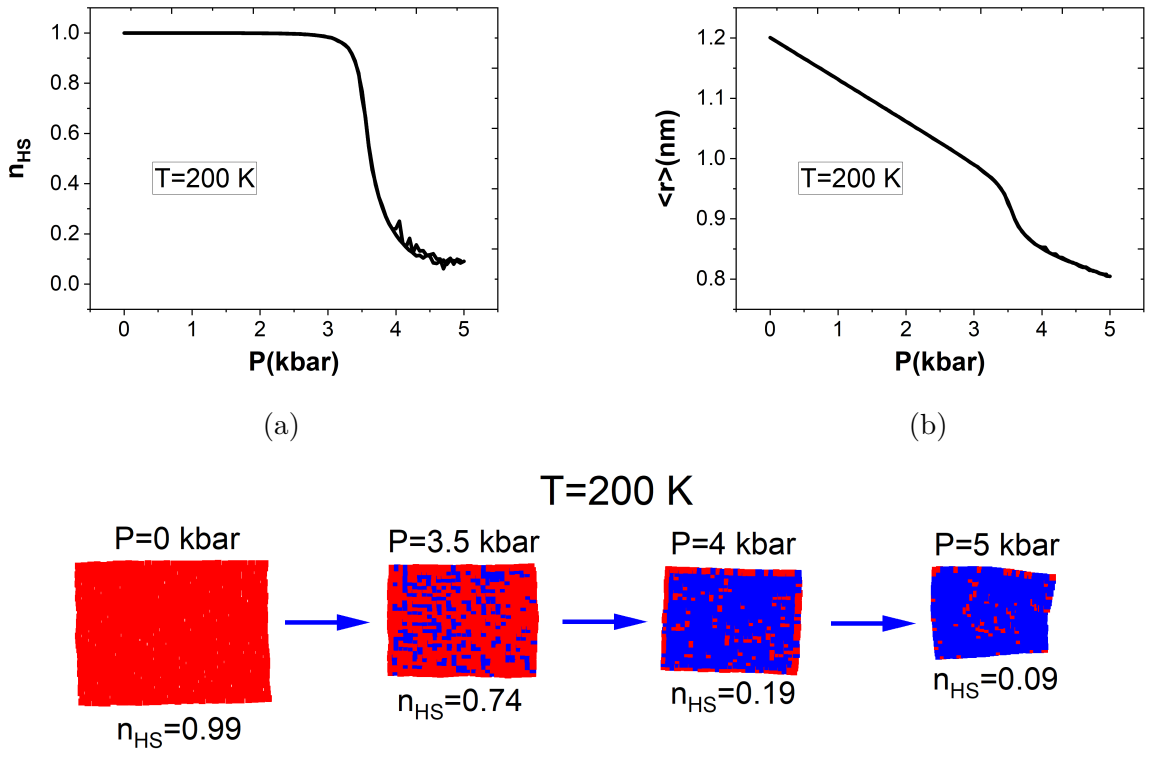

(a) (b)

(c)

Figure 14: Pressure-dependence of the (a) high-spin fraction, n_{HS}, and the (b) average distance, $< r >$, at constant temperature $T = 200$ K showing a gradual spin transition. (c) Selected snapshots showing a ramified structure of the spatial organization of the HS (red dots) and LS (blue dots) sites along the pressure-induced spin transition. The parameter values (except T) are the same as those of Fig. 2

.

B. The Case of two-step baro-switching

When the pressure is applied in the HS phase of Fig. 9a which showed a thermal two-step transition under a constant applied pressure, one may expect to achieve a two-step baro-switching transition at constant temperature. At this end, we performed the simulations for one temperature value, $T = 135$ K where it is expected from Fig. 9a to observe a plateau for pressures $2 \leq P \leq 3$ kbar. The pressure-dependence of the HS fraction, n_{HS}, and average nn distance, $< r >$, are summarized in Figs. 15a and 15b respectively. The associated spin

state configurations along the baro-switching are displayed in Fig. 15c. Figures 15a and 15b clearly exhibit the existence of a double step pressure-induced spin state transition with switching pressure values $P^- = 2$ and $P^+ = 2.5$ kbar.

Both transitions are of first-order, although we do not observe the occurrence of a hysteresis, for the same reasons as those developed for Fig. 13 and also for the slow MC kinetics. Furthermore, the corresponding snapshots, given in Fig. 15c clearly show the presence of a highly organized structure in the form of labyrinth structure leading to the coexistence of HS and LS phases in the plateau region, which are also reminiscent of the patterns obtained in Fig. 11.

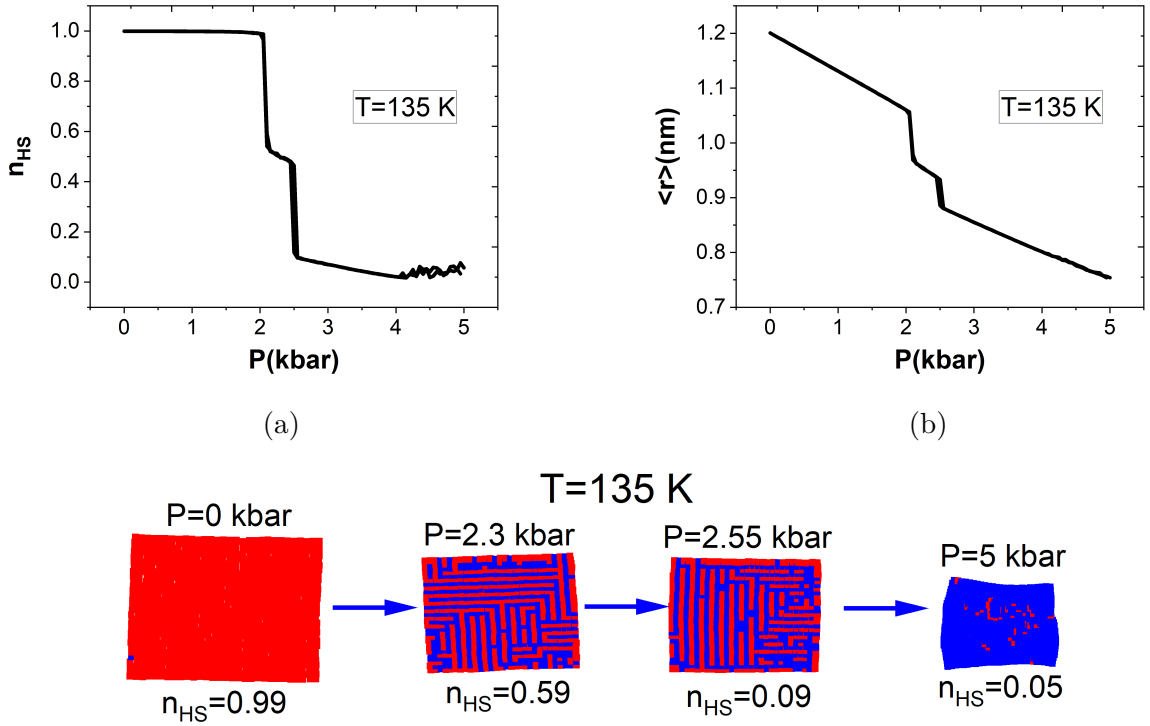

Figure 15: Pressure-dependence of (a) the high-spin fraction, n_{HS}, and (b) average lattice spacing, $< r >$, at constant temperature $T = 135$ K showing the occurrence of two-step transitions. (c) Spatial organization of the HS (red) and LS (blue) states reflecting an alternation of HS and LS stripes along $x-$ and $y-$ directions forming a labyrinth structure. The parameter values (except T) are the same as those Fig. 9.

VI. CONCLUSION

In summary, we used the general genuine electroelastic model to investigate the effect of isotropic applied pressure on the thermodynamic properties of a 2D square lattice. To clarify the consequences of pressure effect on model parameters, we first, propose an analytically treatment of the model in a homogeneous medium allowing to identify the pressure-dependence of equilibrium bond length, the ligand filed energy and elastic constants. Then an effective Hamiltonian is built up by considering the link existing between the distances, elastic constants with the spin states. The find Hamiltonian is solved used Monte Carlo simulations. By monitoring the values of nnn bond length compressibility we could recover almost all the behaviors of HS fraction under pressure, observed experimentally. We analyzed the pressure effect on the elastic interaction parameters and the ligand field contribution as well as on the spatiotemporal behaviors for different cases. When the pressure is null, the usual first-order transitions with single domains nucleation process is obtained as a result of long-range ferroelastic interactions. The formation of the domains takes place from the corners and their propagation to the center of the lattice is accompanied by a distortion of the latter. When applied pressure is non-zero several cases are obtained according to the ratio and the sign between nnn and nn bond compressibilities. The most simple case is one where the hysteresis width vanishes as the pressure increases leading to gradual transition due to the reduction of cooperativity caused by the pressure which prevents the lattice expansion. The second case is that of thermal hysteresis surviving under pressure thanks a subtle competition between the long-and short-range elastic interactions. The snapshots of the self-organized spin states in this case show the formation of domains growing from all corners which turns into a single domain formation from one corner. In the third case, the hysteresis width disappears and reappears once again under pressure exhibiting a reentrant phenomenon which is caused by the non-monotonous behaviour of the elastic interactions. The corresponding spatial distribution of spin sates shows a formation of domains for weak pressure values which disappear beyond threshold pressure value giving rise to a random distribution of spin states and reappear again for strong pressures. The final case concerns the pressure-induced two step transition which is found to be related to the existence of elastic frustration of long-range nature caused by antagonist behaviours of the nn and nnn bond compressibilities. The organization of the spin states in the plateaus showed an

alternation of HS and LS stripes along the longitudinal and vertical directions forming a labyrinth structure which transforms into perfect 1D HS, LS stripes along x-or $y-$directions when one considers anisotropic compressibilities along the previously quoted directions. In addition to the sharp thermal transitions and the rearrangement of the topology of the network interactions induced by the pressure, all these cited behaviors are accompanied by a linear increase of the thermal transition with pressure in good agreement with the available data of literature. Next, the model will be extended to take into account for the effects of the difference in the surface and bulk responses to pressure which will enrich the panoramas of behaviours. Investigations on the 3D systems are also necessary to build more realistic models.

VII. APPENDIX

A. Derivation of the pressure-dependence of the equilibrium distances.

The homogeneous Hamiltonian in cubic symmetry, where for simplicity we only consider nn and nnn interactions, to reduce the number of elastic constants, which themselves are considered as pressure-independent, writes

$$H_{elas} = A\sum_{i,j}\left[x - R(S_i,S_j)\right]^2 + B\sum_{i,k}\left[x\sqrt{2} - d(S_i,S_k)\right]^2 + N\times Px^3 \tag{27}$$

We minimize H_{elas} with respect to x variable, which leads to the following equation,

$$6(A+4B)x - 6(A<R>+4B<d>) + 3Px^2 = 0, \tag{28}$$

where,

$$\begin{aligned} <R> &= \langle R(S_i,S_j\rangle = R_0^{HL} + \frac{\delta R}{2}m \\ <d> &= \langle d(S_i,S_k\rangle = \sqrt{2}(R_0^{HL} + \frac{\delta R}{2}m) \end{aligned} \tag{29}$$

with $m =< S_i >$ is the net "magnetization". Solving the equation of second degree (28) and expanding the solution up to second order in P, by considering the quantity $\frac{(A<R>+2B<d>)P}{(A+2B)^2} \ll 1$, leads to the final expression of the lattice parameter distance, x_{eq}, at mechanical equilibrium,

$$x_{eq} = x_{eq}^0\left(1-\beta\times P\right), \tag{30}$$

where

$$x_{eq}^{0} = \frac{(A < R > +2B < d >)}{(A + 2B)} \tag{31}$$

is the lattice distance at zero pressure and

$$\beta = \frac{(A < R > +2B < d >)}{4\,(A + 2B)^{2}} \tag{32}$$

is the bond compressibility.

B. Expressions of the interacting parameters in Ising version:

It is interesting to remark that the Hamiltonian (27) with homogeneous bond lengths can be developed and re-written under the form of a special Ising model. Replacing the instantaneous distance r_{ij} by x_{eq}, given in equation (30) and inserting the expressions of the lattice bond lengths (2), leads after some longer calculations to the following Ising-like model,

$$H = h(P)\sum_{i}^{N} S_i + J^{nn}(P)\sum_{ij} S_i S_j + J^{nnn}(P)\sum_{ik} S_i S_k + C(m,P). \tag{33}$$

The parameters $h(P)$, $J^{nn}(P)$ and $J^{nnn}(P)$ as well as the constant $C(m,P)$ depend on pressure and their expressions are given below. One can remark in the expression of the effective ligand field, $h(P)$, the ligand field energy is renormalized by the pressure term αP. As a result, the pressure increases the energy gap between the LS and HS states, which is also enhanced by additional elastic field energy contribution resulting from the pressure field created by the nn and nnn sites.

$$J^{nn}(P) = 2A(\frac{\delta R}{4})^{2} \tag{34}$$

$$J^{nnn}(P) = 4B(\frac{\delta R}{4})^{2}, \tag{35}$$

$$h(P) = (\Delta + \alpha P - k_B T \ln g) - \frac{\delta R}{2}(A + 2B)(x_{eq}^{0} - R_{0}^{HL}), \tag{36}$$

where,

$$\alpha = 2x_{eq}^{0}\beta(A + 2B)\left[\left(\frac{\delta R}{4}\right) - (x_{eq}^{0} - R_{0}^{HL})\right]. \tag{37}$$

$$C(m,P) = \frac{zN}{2}\Big(A+2B\Big)\left((x_{eq}^{0})^2\beta^2P^2 + (x_{eq}^{0} - R_0^{HL})^2 + 2\left(\frac{\delta R}{4}\right)^2\right) + NP\left[x_{eq}^{0}\left(1-\beta\right)\right]^3 \tag{38}$$

$$\begin{aligned} C(P) = &\frac{1}{2}\left(N_{nn}A_0(P) + 2N_{nnn}B_0(P)\right)(x - R_{HL})^2 \\ &-\frac{\delta R'}{2}\left[N_{nn}A_1(P) + 2N_{nnn}B_1(P)\right](x - R'_{HL}) + C_0. \end{aligned} \tag{39}$$

VIII. ACKNOWLEDGMENTS

This work was supported by the French-Japan LIA (International Associate Laboratory), the ANR project Mol-CoSM No. ANR-20-CE07-0028-02, the Universities of Versailles and Paris-Saclay-UPSAY, and the CNRS (Centre National de la Recherche Scientifique) and the French Embassy in Sénégal. We thank all of them for their financial support. The authors declare no competing financial interest.

IX. ORCID

Kamel BOUKHEDDADEN: https://orcid.org/0000-0003-0464-1609

Mamadou NDIAYE: https://orcid.org/0000-0001-9370-379X

Bibliography

[1] K. Boukheddaden, M. H. Ritti, G. Bouchez, M. Sy, M. M. Dîrtu, M. Parlier, J. Linares, and Y. Garcia, "Quantitative contact pressure sensor based on spin crossover mechanism for civil security applications," The Journal of Physical Chemistry C, vol. 122, no. 14, pp. 7597–7604, 2018.

[2] O. Kahn and C. J. Martinez, "Spin-Transition Polymers: From Molecular Materials Toward Memory Devices," Science, vol. 279, no. 5347, pp. 44–48, Jan. 1998.

[3] S. P. Vallone, A. N. Tantillo, A. M. dos Santos, J. J. Molaison, R. Kulmaczewski, A. Chapoy, P. Ahmadi, M. A. Halcrow, and K. G. Sandeman, "Giant barocaloric effect at the spin crossover transition of a molecular crystal," Advanced Materials, vol. 31, no. 23, p. 1807334, 2019.

[4] P. J. von Ranke, "A microscopic refrigeration process triggered through spin-crossover mechanism," Applied Physics Letters, vol. 110, no. 18, p. 181909, 2017.

[5] B. Benaicha, K. Van Do, A. Yangui, N. Pittala, A. Lusson, M. Sy, G. Bouchez, H. Fourati, C. J. Gómez-García, S. Triki, and K. Boukheddaden, "Interplay between spin-crossover and luminescence in a multifunctional single crystal iron(ii) complex: towards a new generation of molecular sensors," Chem. Sci., vol. 10, pp. 6791–6798, 2019.

[6] J. Linares, E. Codjovi, and Y. Garcia, "Pressure and temperature spin crossover sensors with optical detection," Sensors, vol. 12, no. 4, p. 4479, 2012.

[7] P. Gütlich, A. Hauser, and H. Spiering, "Thermal and optical switching of iron(II) complexes," Angewandte Chemie-International Edition in english, vol. 33, no. 20, pp. 2024–2054, 1994.

[8] K. Boukheddaden, H. Fourati, Y. Singh, and G. Chastanet, "Evidence of photo-thermal effects on the first-order thermo-induced spin transition of [Fe(NCSe)(py)22(m-bpypz)] spin-crossover material," Magnetochemistry, vol. 5, no. 2, 2019.

[9] G. Chastanet, A. B. Gaspar, J. A. Real, and J.-F. Létard, "Photo-switching spin pairs—synergy between liesst effect and magnetic interaction in an iron(ii) binuclear spin-crossover compound," Chem. Commun., pp. 819–820, 2001.

[10] P. Gütlich and A. Hauser, "Thermal and light-induced spin crossover in iron(ii) complexes," Coordination Chemistry Reviews, vol. 97, pp. 1–22, 1990.

[11] S. Decurtins, P. Gütlich, K. M. Hasselbach, A. Hauser, and H. Spiering, "Light-induced excited-spin-state trapping in iron(ii) spin-crossover systems. optical spectroscopic and magnetic susceptibility study," Inorganic Chemistry, vol. 24, no. 14, pp. 2174–2178, 1985.

[12] J. Krober, E. Codjovi, O. Kahn, F. Groliere, and C. Jay, "A spin transition system with a thermal hysteresis at room temperature," Journal of the American Chemical Society, vol. 115, no. 21, pp. 9810–9811, 1993.

[13] S. W. Biernacki and B. Clerjaud, "Thermally driven low-spin/high-spin phase transitions in solids," Physical Review B, vol. 72, no. 2, 2005.

[14] A. Bousseksou, N. Negre, M. Goiran, L. Salmon, J. P. Tuchagues, M. L. Boillot, K. Boukheddaden, and F. Varret, "Dynamic triggering of a spin-transition by a pulsed magnetic field," Eur. Phys. J. B, vol. 13, no. 3, pp. 451–456, 2000.

[15] T. Mahfoud, G. Molnár, S. Bonhommeau, S. Cobo, L. Salmon, P. Demont, H. Tokoro, S.-I. Ohkoshi, K. Boukheddaden, and A. Bousseksou, "Electric-field-induced charge-transfer

phase transition: A promising approach toward electrically switchable devices," Journal of the American Chemical Society, vol. 131, no. 41, pp. 15 049–15 054, 2009.

[16] D. Pinkowicz, M. Rams, M. Misek, K. V. Kamenev, H. Tomkowiak, A. Katrusiak, and B. Sieklucka, "Enforcing multifunctionality: A pressure-induced spin-crossover photomagnet," Journal of the American Chemical Society, vol. 137, no. 27, pp. 8795–8802, 2015.

[17] V. Ksenofontov, G. Levchenko, H. Spiering, P. Gutlich, J.-F. Letard, Y. Bouhedja, and O. Kahn, "Spin crossover behavior under pressure of fe(pm-l)2(ncs)2 compounds with substituted 2-pyridylmethylene 4-anilino ligands," Chemical Physics Letters, vol. 294, no. 6, pp. 545–553, 1998.

[18] I. Maurin, M. Itoi, J. M. Cain, D. R. Talham, T. Gacoin, K. Boukheddaden, and J.-P. Itié, "High-pressure behavior of heteroepitaxial core–shell particles made of prussian blue analogs," Journal of Applied Physics, vol. 129, no. 23, p. 235106, 2021.

[19] J. M. Cain, W. He, I. Maurin, M. W. Meisel, and D. R. Talham, "Stimulus induced strain in spin transition heterostructures," Journal of Applied Physics, vol. 129, no. 16, p. 160903, 2021.

[20] P. Gütlich, V. Ksenofontov, and A. B. Gaspar, "Pressure effect studies on spin crossover systems," Coordination Chemistry Reviews, vol. 249, no. 17, pp. 1811–1829, 2005.

[21] C.-M. Jureschi, I. Rusu, E. Codjovi, J. Linares, Y. Garcia, and A. Rotaru, "Thermo- and piezochromic properties of [fe(hyptrz)]a2 · h2o spin crossover 1d coordination polymer: Towards spin crossover based temperature and pressure sensors," Physica B: Condensed Matter, vol. 449, pp. 47–51, 2014.

[22] J. Laisney, H. J. Shepherd, L. Rechignat, G. Molnár, E. Rivière, and M.-L. Boillot, "Pressure-induced switching properties of the iron(iii) spin-transition complex [feiii(3-omesaleen)$_2$]pf$_6$," Phys. Chem. Chem. Phys., vol. 20, pp. 15 951–15 959, 2018.

[23] A. B. Gaspar, G. Molnár, A. Rotaru, and H. J. Shepherd, "Pressure effect investigations on spin-crossover coordination compounds," Comptes Rendus Chimie, vol. 21, no. 12, pp. 1095–1120, 2018.

[24] H. Oyanagi, T. Tayagaki, and K. Tanaka, "Synchrotron radiation study of photo-induced spin-crossover transitions: Microscopic origin of nonlinear phase transition," Journal of Luminescence, vol. 119-120, pp. 361–369, 2006, dynamical Processes in Excited States of Solids.

[25] P. Gütlich and H. Goodwin, "Spin crossover - An overall perspective," in Spin crossover in transition metal compounds I, ser. Topics in Current Chemistry, 2004, vol. 233, pp. 1–47.

[26] P. Guionneau, "Crystallography and spin-crossover. a view of breathing materials," Dalton Trans., vol. 43, pp. 382–393, 2014.

[27] J. A. Wolny, V. Schünemann, Z. Németh, and G. Vankó, "Spectroscopic techniques to characterize the spin state: Vibrational, optical, mössbauer, nmr, and x-ray spectroscopy," Comptes Rendus Chimie, vol. 21, no. 12, pp. 1152–1169, 2018.

[28] K. Boukheddaden, M. Sy, M. Paez-Espejo, A. Slimani, and F. Varret, "Dynamical control of the spin transition inside the thermal hysteresis loop of a spin-crossover single crystal," Physica B, vol. 486, pp. 187–191, 2016.

[29] M. Castro, O. Roubeau, L. Piñeiro-López, J. A. Real, and J. A. Rodríguez-Velamazán, "Pulsed-laser switching in the bistability domain of a cooperative spin crossover compound: A critical study through calorimetry," The Journal of Physical Chemistry C, vol. 119, no. 30, pp. 17 334–17 343, 2015.

[30] A. G. Maddock and J. J. Schleiffer, "Spin cross-over and the mössbauer emission spectrum of cobalt-57-labelled di-isothiocyanatobis(1,10-phenanthroline)-iron(ii) and -cobalt(ii)," J. Chem. Soc., Dalton Trans., pp. 617–620, 1977.

[31] N. N. Adarsh, M. M. Dîrtu, A. Rotaru, and Y. Garcia, "57Fe Mössbauer spectroscopy study of a 2D spin transition coordination polymer built from a tris-1R-tetrazole ligand," Hyperfine Interactions, vol. 238, p. 60, 2017.

[32] A. Marino, M. Servol, R. Bertoni, M. Lorenc, C. Mauriac, J.-F. Létard, and E. Collet, "Femtosecond optical pump–probe reflectivity studies of spin-state photo-switching in the spin-crossover molecular crystals [fe(pm-aza)2(ncs)2]," Polyhedron, vol. 66, pp. 123–128, 2013, iCMM 2012.

[33] G.-M. Rotaru, E. Codjovi, P.-R. Dahoo, I. Maurin, J. Linares, and A. Rotaru, "Monitoring spin-crossover properties by diffused reflectivity," Symmetry, vol. 13, no. 7, 2021.

[34] M. Sy, F. Varret, K. Boukheddaden, G. Bouchez, J. Marrot, S. Kawata, and S. Kaizaki, "Structure-driven orientation of the high-spin–low-spin interface in a spin-crossover single crystal," Angewandte Chemie International Edition, vol. 53, no. 29, pp. 7539–7542, 2014.

[35] S. Pillet, J. Hubsch, and C. Lecomte, "Single crystal diffraction analysis of the thermal spin

conversion in [fe(btr)$_2$(ncs)$_2$](h$_2$o): evidence for spin-like domain formation," Eur. Phys. J. B, vol. 38, no. 4, pp. 541–552, 2004.

[36] Y. Garcia, F. Robert, A. D. Naik, G. Zhou, B. Tinant, K. Robeyns, S. Michotte, and L. Piraux, "Spin transition charted in a fluorophore-tagged thermochromic dinuclear iron(ii) complex," Journal of the American Chemical Society, vol. 133, no. 40, pp. 15 850–15 853, 2011.

[37] C. Lochenie, K. Schötz, F. Panzer, H. Kurz, B. Maier, F. Puchtler, S. Agarwal, A. Köhler, and B. Weber, "Spin-crossover iron(ii) coordination polymer with fluorescent properties: Correlation between emission properties and spin state," Journal of the American Chemical Society, vol. 140, no. 2, pp. 700–709, 2018.

[38] M. Estrader, J. Salinas Uber, L. A. Barrios, J. Garcia, P. Lloyd-Williams, O. Roubeau, S. J. Teat, and G. Aromí, "A magneto-optical molecular device: Interplay of spin crossover, luminescence, photomagnetism, and photochromism," Angewandte Chemie International Edition, vol. 56, no. 49, pp. 15 622–15 627, 2017.

[39] F. Varret, C. Chong, A. Slimani, D. Garrot, Y. Garcia, and A. D. Naik, Real-Time Observation of Spin-Transitions by Optical Microscopy. John Wiley & Sons Ltd, 2013, pp. 425–441.

[40] T. Togo, S. A. Amolegbe, R. Yamaguchi, T. Kuroda-Sowa, M. Nakaya, K. Shimayama, M. Nakamura, and S. Hayami, "Crystal structure and spin-crossover behavior of iron(iii) complex with nitroprusside," Chemistry Letters, vol. 42, no. 12, pp. 1542–1544, 2013.

[41] J. Krober, E. Codjovi, O. Kahn, F. Groliere, and C. Jay, "A spin transition system with a thermal hysteresis at room temperature," Journal of the American Chemical Society, vol. 115, no. 21, pp. 9810–9811, 1993.

[42] O. Roubeau, "Triazole-based one-dimensional spin-crossover coordination polymers," Chemistry – A European Journal, vol. 18, no. 48, pp. 15 230–15 244, 2012.

[43] N. Moliner, C. Muñoz, S. Létard, X. Solans, N. Menéndez, A. Goujon, F. Varret, and J. A. Real, "Spin Crossover Bistability in Three Mutually Perpendicular Interpenetrated (4,4) Nets," Inorganic Chemistry, vol. 39, no. 23, pp. 5390–5393, Nov. 2000.

[44] P. J. van Koningsbruggen, Y. Garcia, O. Kahn, L. Fournes, H. Kooijman, A. L. Spek, J. G. Haasnoot, J. Moscovici, K. Provost, A. Michalowicz, F. Renz, and P. Gütlich, "Synthesis, crystal structure, exafs, and magnetic properties of catena [tris(1,2-bis(tetrazol-1-yl)propane-n1,n1)iron(ii)] bis(perchlorate). first crystal structure of an iron(ii) spin-crossover chain compound," Inorganic Chemistry, vol. 39, no. 9, pp. 1891–1900, 2000.

[45] Z.-Y. Li, J.-W. Dai, Y. Shiota, K. Yoshizawa, S. Kanegawa, and O. Sato, "Multi-step spin crossover accompanied by symmetry breaking in an feiii complex: Crystallographic evidence and dft studies," Chemistry – A European Journal, vol. 19, no. 39, pp. 12 948–12 952, 2013.

[46] C. J. Adams, M. C. Muñoz, R. E. Waddington, and J. A. Real, "Cooperative spin transition in the two-dimensional coordination polymer [fe(4,4-bipyridine)2(ncx)2] · 4chcl3 (x = s, se)," Inorganic Chemistry, vol. 50, no. 21, pp. 10 633–10 642, 2011.

[47] C.-J. Zhang, K.-T. Lian, G.-Z. Huang, S. Bala, Z.-P. Ni, and M.-L. Tong, "Hysteretic four-step spin-crossover in a 3d hofmann-type metal–organic framework with aromatic guest," Chem. Commun., vol. 55, pp. 11 033–11 036, 2019.

[48] Z.-Y. Li, H. Ohtsu, T. Kojima, J.-W. Dai, T. Yoshida, B. K. Breedlove, W.-X. Zhang, H. Iguchi, O. Sato, M. Kawano, and M. Yamashita, "Direct Observation of Ordered High-Spin-Low-Spin Intermediate States of an Iron(III) Three-Step Spin-Crossover Complex," Angewandte Chemie, vol. 128, no. 17, pp. 5270–5275, Apr. 2016.

[49] C. P. Slichter and H. G. Drickamer, "Pressure-induced electronic changes in compounds of iron," The Journal of Chemical Physics, vol. 56, no. 5, pp. 2142–2160, 1972.

[50] W. Kosaka, H. Tokoro, T. Matsuda, K. Hashimoto, and S.-i. Ohkoshi, "Extremely gradual spin-crossover phenomenon in a cyano-bridged fe-mo bimetallic assembly," The Journal of Physical Chemistry C, vol. 113, no. 35, pp. 15 751–15 755, 2009.

[51] H. Spiering and N. Willenbacher, "Elastic interaction of high-spin and low-spin complex molecules in spin-crossover compounds.ii," J. Phys.: Condens. Matter, vol. 1, no. 50, pp. 10 089–10 105, 1989.

[52] J. Wajnflasz and R. Pick, "Transition low spin high spindans les complexes de Fe $^{2+}$," Le Journal de Physique Colloques, vol. 32, no. C1, pp. C1–91–C1–92, Feb. 1971.

[53] K. Boukheddaden, J. Linares, E. Codjovi, F. Varret, V. Niel, and J. A. Real, "Dynamical ising-like model for the two-step spin-crossover systems," Journal of Applied Physics, vol. 93, no. 10, pp. 7103–7105, 2003.

[54] S. Miyashita, Y. Konishi, M. Nishino, H. Tokoro, and P. A. Rikvold, "Realization of the mean-field universality class in spin-crossover materials," Phys. Rev. B, vol. 77, p. 014105, Jan 2008.

[55] A. Bousseksou, F. Varret, and J. Nasser, "Ising-like model for the two step spin-crossover of binuclear molecules," Journal de Physique I, vol. 3, no. 6, pp. 1463–1473, Jun. 1993.

[56] J. A. Nasser, K. Boukheddaden, and J. Linares, "Two-step spin conversion and other effects in the atom-phonon coupling model," The European Physical Journal B - Condensed Matter and Complex Systems, vol. 39, no. 2, pp. 219–227, May 2004.

[57] W. Nicolazzi, S. Pillet, and C. Lecomte, "Two-variable anharmonic model for spin-crossover solids: A like-spin domains interpretation," Phys. Rev. B, vol. 78, p. 174401, Nov 2008.

[58] C. Fourmental, S. Mondal, R. Banerjee, A. Bellec, Y. Garreau, A. Coati, C. Chacon, Y. Girard, J. Lagoute, S. Rousset, M.-L. Boillot, T. Mallah, C. Enachescu, C. Barreteau, Y. J. Dappe, A. Smogunov, S. Narasimhan, and V. Repain, "Importance of epitaxial strain at a spin-crossover molecule–metal interface," The Journal of Physical Chemistry Letters, vol. 10, no. 14, pp. 4103–4109, 2019, pMID: 31265299.

[59] C. Enachescu, M. Nishino, S. Miyashita, L. Stoleriu, and A. Stancu, "Monte carlo metropolis study of cluster evolution in spin-crossover solids within the framework of a mechanoelastic model," Phys. Rev. B, vol. 86, p. 054114, Aug 2012.

[60] M. Ndiaye, N. E. I. Belmouri, J. Linares, and K. Boukheddaden, "Elastic origin of the unsymmetrical thermal hysteresis in spin crossover materials: Evidence of symmetry breaking," Symmetry, vol. 13, no. 5, 2021.

[61] M. Ndiaye, Y. Singh, H. Fourati, M. Sy, B. Lo, and K. Boukheddaden, "Isomorphism between the electro-elastic modeling of the spin transition and ising-like model with competing interactions: Elastic generation of self-organized spin states," Journal of Applied Physics, vol. 129, no. 15, p. 153901, 2021.

[62] A. Slimani, K. Boukheddaden, and K. Yamashita, "Effect of intermolecular interactions on the nucleation, growth, and propagation of like-spin domains in spin-crossover materials," Physical Review B, vol. 92, no. 1, p. 014111, 2015.

[63] R. Li, G. Levchenko, F. J. Valverde-Muñoz, A. B. Gaspar, V. V. Ivashko, Q. Li, B. Liu, M. Yuan, H. Fylymonov, and J. A. Real, "Pressure tunable electronic bistability in fe(ii) hofmann-like two-dimensional coordination polymer [fe(fpz)2pt(cn)4]: A comprehensive experimental and theoretical study," Inorganic Chemistry, vol. 60, no. 21, pp. 16 016–16 028, 2021.

[64] I. V. Gudyma, A. I. Maksymov, and V. V. Ivashko, "Study of pressure influence on thermal transition in spin-crossover nanomaterials," Nanoscale Research Letters, vol. 9, no. 1, p. 691, Dec. 2014.

[65] Y. Konishi, H. Tokoro, M. Nishino, and S. Miyashita, "Monte carlo simulation of pressure-induced phase transitions in spin-crossover materials," Phys. Rev. Lett., vol. 100, p. 067206, 2008.

[66] A. Rotaru, F. Varret, E. Codjovi, K. Boukheddaden, J. Linares, A. Stancu, P. Guionneau, and J.-F. Letard, "Hydrostatic pressure investigation of the spin crossover compound [fe(pm-bia)2(ncs)2] polymorph i using reflectance detection," Journal of Applied Physics, vol. 106, no. 5, p. 053515, 2009.

[67] K. Babilotte and K. Boukheddaden, "Theoretical investigations on the pressure effects in spin-crossover materials: Reentrant phase transitions and other behavior," Phys. Rev. B, vol. 101, p. 174113, May 2020.

[68] H.-Z. Ye, C. Sun, and H. Jiang, "Monte-carlo simulations of spin-crossover phenomena based on a vibronic ising-like model with realistic parameters," Phys. Chem. Chem. Phys., vol. 17, pp. 6801–6808, 2015.

[69] E. König, G. Ritter, J. Waigel, and H. A. Goodwin, "The effect of pressure on the thermal hysteresis of the first-order spin transition in bis(1,10-phenanthroline-2-carbaldehyde phenylhydrazone) iron (ii) complexes," The Journal of Chemical Physics, vol. 83, no. 6, pp. 3055–3061, 1985.

[70] M. Reczyński, D. Pinkowicz, K. Nakabayashi, C. Näther, J. Stanek, M. Kozieł, J. Kalinowska-Tłuścik, B. Sieklucka, S.-i. Ohkoshi, and B. Nowicka, "Room-temperature bistability in a ni–fe chain: Electron transfer controlled by temperature, pressure, light, and humidity," Angewandte Chemie International Edition, vol. 60, no. 5, pp. 2330–2338, 2021.

[71] H. Spiering, K. Boukheddaden, J. Linares, and F. Varret, "Total free energy of a spin-crossover molecular system," Phys. Rev. B, vol. 70, p. 184106, Nov 2004.

[72] Y. Li, A. Benchohra, B. Xu, B. Baptiste, K. Béneut, P. Parisiades, L. Delbes, A. Soyer, K. Boukheddaden, and R. Lescouëzec, "Pressure-induced conversion of a paramagnetic feco complex into a molecular magnetic switch with tuneable hysteresis," Angewandte Chemie International Edition, vol. 59, no. 39, pp. 17 272–17 276, 2020.

[73] C. Lecourt, Y. Izumi, K. Maryunina, K. Inoue, N. Bélanger-Desmarais, C. Reber, C. Desroches, and D. Luneau, "Hypersensitive pressure-dependence of the conversion temperature of hysteretic valence tautomeric manganese–nitronyl nitroxide radical 2d-frameworks," Chem. Commun., vol. 57, pp. 2376–2379, 2021.

[74] S. Hayami, Amphiphilic and Liquid Crystalline Spin-Crossover Complexes. John Wiley and Sons, Ltd, 2013, ch. 12, pp. 321–345.

[75] D. Taniguchi, J. Okabayashi, and C. Hotta, "Pressure-induced two-step spin crossover in a double-layered elastic model," Phys. Rev. B, vol. 96, p. 174104, Nov 2017.

[76] H. J. Shepherd, S. Bonnet, P. Guionneau, S. Bedoui, G. Garbarino, W. Nicolazzi, A. Bousseksou, and G. Molnár, "Pressure-induced two-step spin transition with structural symmetry breaking: X-ray diffraction, magnetic, and raman studies," Phys. Rev. B, vol. 84, p. 144107, Oct 2011.

[77] M. Yuan, R. Li, Q. Li, L. Berezhnaya, H. Fylymonov, M. Seredyuk, N. Liedienov, J. A. Real, and G. Levchenko, "Pressure and Thermally Induced Spin Crossover in a 2D Iron(II) Coordination Polymer {Fe[bipy(ttr)2]}n," in 2021 5th IEEE Electron Devices Technology & Manufacturing Conference (EDTM). Chengdu, China: IEEE, Apr. 2021, pp. 1–3.

[78] N. Paradis, F. Le Gac, P. Guionneau, A. Largeteau, D. Yufit, P. Rosa, J.-F. Létard, and G. Chastanet, "Effects of Internal and External Pressure on the [Fe(PM-PEA)2(NCS)2] Spin-Crossover Compound (with PM-PEA = N-(2-pyridylmethylene)-4-(phenylethynyl)aniline)," Magnetochemistry, vol. 2, no. 1, p. 15, Mar. 2016.

[79] S. Wang, S. Hirai, M. C. Shapiro, S. C. Riggs, T. H. Geballe, W. L. Mao, and I. R. Fisher, "Pressure-induced symmetry breaking in tetragonal $csaui_3$," Phys. Rev. B, vol. 87, p. 054104, Feb 2013.

[80] J. Jeftic, H. Romstedt, and A. Hauser, "The interplay between the spin transition and the crystallographic phase transition in the fe(ii) spin-crossover system [zn1-xfex(ptz)6](bf4)2 (x = 0.1, 1,ptz=1-propyltetrazole)," Journal of Physics and Chemistry of Solids, vol. 57, no. 11, pp. 1743–1750, 1996.

[81] T. Granier, B. Gallois, J. Gaultier, J. A. Real, and J. Zarembowitch, "High-pressure single-crystal x-ray diffraction study of two spin-crossover iron(ii) complexes: Fe(phen)2(ncs)2 and fe(btz)2(ncs)2," Inorganic Chemistry, vol. 32, no. 23, pp. 5305–5312, 1993.

[82] A. Tissot, H. J. Shepherd, L. Toupet, E. Collet, J. Sainton, G. Molnár, P. Guionneau, and M.-L. Boillot, "Temperature- and pressure-induced switching of the molecular spin state of an orthorhombic iron(iii) spin-crossover salt," European Journal of Inorganic Chemistry, vol. 2013, no. 5-6, pp. 1001–1008, 2013.

[83] E. Milin, V. Patinec, S. Triki, E.-E. Bendeif, S. Pillet, M. Marchivie, G. Chastanet, and

K. Boukheddaden, "Elastic frustration triggering photoinduced hidden hysteresis and multistability in a two-dimensional photoswitchable hofmann-like spin-crossover metal organic framework," Inorganic Chemistry, vol. 55, no. 22, pp. 11 652–11 661, 2016.

[84] J. Jung, F. Bruchhäuser, R. Feile, H. Spiering, and P. Gütlich, "The cooperative spin transition in [FexZn1-x(ptz)$_6$](BF$_4$)^2: I. Elastic properties-an oriented sample rotation study by Brillouin spectroscopy," Zeitschrift für Physik B Condensed Matter, vol. 100, no. 4, pp. 517–522, 1996.

[85] G. G. Levchenko, A. V. Khristov, and V. N. Varyukhin, "Spin crossover in iron(ii)-containing complex compounds under a pressure (review article)," Low Temperature Physics, vol. 40, no. 7, pp. 571–585, 2014.

[86] A. Desaix, O. Roubeau, J. Jeftic, J. G. Haasnoot, K. Boukheddaden, E. Codjovi, J. Linarès, M. Noguès, and F. Varret, "Light-induced bistability in spin transition solids leading to thermal and optical hysteresis," The European Physical Journal B - Condensed Matter and Complex Systems, vol. 6, no. 2, pp. 183–193, 1998.